DISS. ETH NO. 18501

ADDRESSING CLINICAL NEEDS OF THE AORTIC ROOT AND CORONARY ARTERIES THROUGH THE USE OF COMPUTATIONAL FLUID DYNAMICS AND COMPUTED TOMOGRAPHY

A dissertation submitted to the

SWISS FEDERAL INSTITUTE OF TECHNOLOGY ZURICH

for the degree of

DOCTOR OF SCIENCES

presented by

Joseph A. Knight
Masters of Engineering Science,
University of South Florida, Tampa

Born on December 26th, 1978
citizen of The United States of America

accepted on the recommendation of

Prof. Dr. Dimos Poulikakos, examiner
Dr. Vartan Kurtcuoglu, co-examiner
Dr. William Marshall, co-examiner

Zurich, 2009

II

III

"This is the true joy in life,
being used for a purpose recognized by yourself as a mighty one.
Being a force of nature instead of a feverish, selfish little clod of ailments and grievances,
complaining that the world will not devote itself to making you happy.
I am of the opinion that my life belongs to the whole community
and as long as I live, it is my privilege to do for it what I can.
I want to be thoroughly used up when I die,
for the harder I work, the more I live.
I rejoice in life for its own sake.
Life is no brief candle to me.
It is a sort of splendid torch which I have got hold of for the moment
and I want to make it burn as brightly as possible
before handing it on to future generations."

- George Bernard Shaw

"It is not the critic who counts:
not the man who points out how the strong man stumbles
or where the doer of deeds could have done better.
The credit belongs to the man who is actually in the arena,
whose face is marred by dust and sweat and blood,
who strives valiantly,
who errs and comes up short again and again,
because there is no effort without error or shortcoming,
but who knows the great enthusiasms, the great devotions,
who spends himself for a worthy cause;
who, at the best, knows, in the end, the triumph of high achievement,
and who, at the worst, if he fails,
at least he fails while daring greatly,
so that his place shall never be with those cold and timid souls
who knew neither victory nor defeat."

- Theodore Roosevelt
"*Citizenship in a Republic*"
Speech at the Sorbonne,
Paris, April 23, 1910

Acknowledgments

To pursue a doctorate is to put one's skills and thinking to a focused area and research it to a level of understanding that very few others have acquired. To have the opportunity to thoroughly delve into a subject area, and to become an expert in an extremely focused area, is truly a luxury, and indeed a joyous experience.

The present dissertation was realized in the Laboratory of Thermodynamics in Emerging Technologies (LTNT) at the ETH Zurich, in cooperation with the Institute for Diagnostic Radiology at the University Hospital Zurich, and would not have been possible without the scientific, technical, financial and moral support of numerous people. Consequently, there are numerous people and institutions for which I am thankful for allowing me this luxury.

I first must thank Prof. Poulikakos who has given me the opportunity to perform research as part of the LTNT. The freedom Prof. Poulikakos gives his PhD students to explore and find their path through the particular research problem that they have undertaken is truly one of the greatest gifts we members of LTNT receive. Yet, still Prof. Poulikakos is always there to help guide each of us, and when need be motivate us, to ensure that we are not just wondering down dead end paths of knowledge that will never produce any worthy result. The balance of these two makes for an excellent environment to work through challenging issues that have never been tackled before, while always knowing that there is support and assistance nearby.

I would also like to thank Prof. Poulikakos for the opportunity to be involved in the lab in multiple capacities outside of my research. As the webmaster for nearly my entire time at the LTNT I have had the opportunity to always be abreast of what is going on in the lab, while also affording me the chance to work one-on-one with the different members of LTNT. As the Capitan of the LTNT SOLA fourteen person relay through the three mountains that surround Zurich, I was able to work with and get to know the members of the lab in my personally enjoyable past time of running. Thank you to all the members of the LTNT SOLA teams over the past three years. Though at times we were "Lost and Delirious", we always ran "Like There's No Tomorrow", and it all ended up being a bunch of "Hot and Cool Science" in the end.

Next up, the "Bio group" – including past members (Evangelos Boutsianis and Sumeet Gupta), those that were with me through most, or in some cases all, of my work (Fraser Callaghan, Doro

Hollnagel, Vartan Kurtcuoglu, Anastasios Marmaras and Ufuk Olgac) and those that have more recently become part of the lab (Simone Bottan and Bercan Siyahhan) – You all are great. Though at times we could be bombarded with meetings and presentations, it was always the free flowing Bio-group meetings that I looked forward to the most. These meetings provided an outlet for me to present a particularly vexing problem I was stumped by and, more than once, to come away with the perfect solution, or at a minimum, a ton of new ideas and possible work-arounds to try.

In particular, special thanks goes to Vartan, the Bio-group team leader, for all of his input and assistance in making my research and manuscripts their best. Your ability to teach, by stepping into the student's knowledge base and presenting in a manner that he/she might best understand, was tremendously helpful to me innumerable times throughout the work for my dissertation. Fraser and Doro, thank you for all of your help with the writing of my Tecplot and Matlab scripts. Doro you were always a tremendous help in making sure that all of my numbers and equations were accurate. I also enjoyed hanging out with you and Marc – especially our trips to Desperados!

A very special thanks goes to Ufuk who I worked closely with throughout my research, sharing meshes, manuscripts, and an office while working under the same CO-Me project – Good times on the U.S. West Coast my friend. Stefan Saur was also part of CO-Me project 12, and played a crucial part in providing the models from computed tomography for the patients used in my research. Thanks for always being a "Skype instant message" away for me to ask the last minute question or get clarification on something. Of course, I am deeply grateful for the financial support given by the Swiss National Science Foundation through CO-Me, without which my work would not have been possible, but I also appreciate having the chance to be part of such a vastly innovative group of people that have been collected together for such diverse biomedical engineering projects.

Biomedical engineering research is by its nature a multi-disciplinary area requiring the input of numerous fields, and in particular, input from the medical domain. I was exceptionally fortunate to have such incredible access to a great group of physicians at the University hospital in Zurich. I very much appreciated being able to just cross the street and head over to the hospital to get specific questions answered – and Hatem was always there with a response or some guidance to push me in the right direction; at points in my research these were daily trips. Lotus, and the tremendous amount of patient data you collected for my work was a tremendous help. You were also always available for questions, and to help me figure out where in the hospital Hatem might be hiding. It was great working with Paul on the two manuscripts concerning the locations of the coronary arteries in both healthy and diseased patients. I also received great medical input from Dr. William Marshall, a retired cardiac surgeon, who is

currently the Associate Dean of Clinical Affairs and Venture Development at the University of South Florida in the U.S. He has played numerous pivotal roles in my reaching of new heights that I never thought possible. I greatly appreciate all of your medical insights and input throughout my doctoral work, but even more so for your tremendous assistance that has put me in such an incredible place in my career, and in life.

The LTNT is composed of multiple disciplines, which afforded me the opportunity to be exposed to not only some interesting research that I would likely have never sought out on my own – thermo, nano, fuel cells, etc. – but also gave me the chance to meet some more great people. You all provided a great break when I wanted to get away from my own research or for great adventures when we were not in the office – though I could do without the cliff falling. I would like to specifically thank Christian Weinmueller for his involvement and enthusiasm in the many crazy projects we worked on, explored, and delved into, outside of the office. I have many great memories hanging out with you and Sonja.

Thanks to all of the German native speakers that helped me with the writing of my "Zusammenfassung". I think by the end we had every native speaker in the lab take a look through it. I greatly appreciate your assistance in this.

I had a tremendous opportunity to explore an aspect of bioengineering that I have always been fascinated with, but had never had the chance to really get a "pipette into my hands". That all changed with iGEM – the international genetically engineered machine competition held at MIT. My great gratitude goes to Dr. Sven Panke and Dr. Joerg Stelling for allowing me to be one the members to represent the ETH in the competition. Thank you to all of the 2007 ETH iGEM members for some great times and a great presentation that allowed us to bring home the first place presentation trophy!

I would like to thank the many people outside of LTNT that I was able to become friends with during my time in Switzerland– Benedicte, Christos, Dani, Guido, Nadja, Nati, Peter, Philipp, Marc, Silvia, Tina, and anyone else that I did not list, but you know who you are. For an American to leave Freedom-land and spend three years in a new place is certainly a horizon broadening and eye opening experience. Yet, it can also bring with it many trials in missing friends, family and the familiarity of those things that we all seem to take for granted when we are comfortably secure in them. Each of you helped to make it all better for me and at some points, as hard as it might be to believe, you all helped to make "here" feel a bit like home.

Finally, for anyone reading this hoping that I might part some great wisdom on the secret of how to complete the doctoral work in three years (as it will have been exactly three years from my start day (July 4th, 2006) till my defense (July 3rd, 2009) – if you add in the day from the 2008 leap year). Well, unfortunately I must delivery some bad news – there is no such secret! In fact, my advice to you – don't try it! You will end up working just as many hours as if you were here for 3.5 to 4 years any way (say good bye weekends, holidays, and nights) and you will be stressed out of your mind. No, no… it is much better to take your time, get out and enjoy the wonderful country that Switzerland is, including the phenomenal city of Zurich (which was voted #1 city in the world to live in all three years I was here); and to really get to know and take pleasure in the many adventures you should partake in with the other members of the LTNT.

Thank You All; & All the Best!

Summary

Diseases of the cardiovascular system are the number one cause of death in most developed nations. With the ever increasing population size and life expectancy, combined with changes in the lifestyle and nutritional habits of those in rapidly developing countries, this trend will only become more of a burden to the healthcare systems throughout the world in the coming decades.

These diseases, and their treatments, are numerous, complex, and not entirely understood. A multi-disciplinary approach has proven to be the most successful means of tackling these challenges. This work focuses on combining the tools of the radiologist (such as computed tomography (CT)), the biomedical engineer (such as computational fluid dynamics (CFD)) and the computer scientist (such as the use of parallel processing) to better understand and treat diseases of the aortic root and the coronary arteries of the human heart.

Accurate knowledge of the anatomy of interest is crucial in understanding and treating diseases of the cardiovascular system. All current measurements of the coronary artery ostia as they originate from the aortic root have been performed in cadaver specimens, and not in the under pressure aortic root in which treatment protocols are performed. A comparison between measurements taken of the coronary ostial origins in this high pressure native environment, through the use of CT, to those taken of cadaveric hearts, demonstrates a significant difference regarding the right coronary artery (RCA). Large variations of both right and left coronary ostia origins emphasize the importance of considering such anatomic variations in the development of treatments; for example the recent advent of percutaneous aortic valve replacement and its associated complications of obstruction of the coronary ostia.

Diseases of the aortic root, and specifically the ascending aorta and/or sinuses of Valsalva, such as aneurysm or dissection, can have disastrous results on patient outcomes. Fortunately, surgical techniques have been developed to treat such diseases. Through the use of CT and CFD, the resulting fluid flow parameters of two such techniques for the replacement of the ascending aorta – with a pseudo-sinus graft and a technique referred to as the Cabrol procedure – are compared to those of the normal aortic root anatomy. CFD

results for the Cabrol procedure, indicating low flow rates into the right coronary artery, correlate well with clinical and CT follow-up of seven patients having undergone the Cabrol procedure that had a higher incidence of occlusion in the right, as compared to the left, Cabrol graft at long-term follow-up. Based on the higher rate of occlusions of the RCA and the unique flow into the Cabrol graft found in the CFD analysis, together with a patent RCA of all directly attached coronaries in the Cabrol group follow-up, this study suggests the use of a direct connection whenever feasible. These preliminary data warrant further investigation.

The first branches of the aorta are the two coronary arteries that supply the heart itself. It is believed that the hemodynamic parameters of wall shear, such as – average wall shear stress (AWSS), average wall shear stress gradient (AWSSG), oscillatory shear index (OSI) and residence residual time (RRT) – predict areas vulnerable to plaque formation that can lead to atherosclerosis. These parameters, from CFD analysis of the patients' vessels before the onset of atherosclerosis, are correlated to the specific plaque sites thereafter. An analysis of each parameters' sensitivity and positive predictive value (PPV) is also performed.

For the RCA, AWSS with its higher sensitivity than OSI, as well as its simple calculation, is found to be the parameter best suited for potential clinical use when the most number of plaques are to be found, irrespective of the number of false-positives. RRT and OSI, with their significantly higher PPV than the other two parameters, are found to be the parameters best suited for those clinical applications of the RCA in which the number of false positives is to be minimized.

With its significantly higher sensitivity than all three other parameters, AWSS is also the parameter of choice for the LCA when the largest number of plaques needs to be identified with little regard for false-positives. RRT, with its significantly higher PPV than AWSS, AWSSG and OSI is the parameter best suited for clinical applications of the left coronary artery when the number of false-positives is to be minimized.

Future studies should investigate possible combined parameters that maintain the high sensitivity of AWSS, while also having the high PPV of RRT.

Zusammenfassung

In den meisten Industrieländern sind Erkrankungen des Herz-Kreislaufsystems die häufigste Todesursache. Zudem werden Bevölkerungswachstum, steigende Lebenserwartung und die sich verändernden Lebens- und Ernährungsgewohnheiten in den Entwicklungsländern in den nächsten Jahrzehnten zu einem globalen Anstieg dieser Erkrankungen beitragen und somit die nationalen Gesundheitssysteme noch stärker belasten.

Viele Herz-Kreislauferkrankungen und ihre Behandlungsmethoden sind hochkomplex und daher noch nicht umfassend untersucht. Zur Erforschung dieser Erkrankungen haben sich multidisziplinäre Ansätze als vielversprechend erwiesen. In der vorliegenden Arbeit wird die Methodik des Radiologen (die Computertomographie (CT)), des Ingenieurs (numerische Strömungsberechnung (CFD)) und des Informatikers (gesteigerte Rechnerleistung) kombiniert, um die Erkrankungen der Aortenwurzel und der Herzkranzgefässe (Koronararterien) am menschlichen Herzen besser zu verstehen und behandeln zu können.

Dabei ist die Kenntnis über die Anatomie der Gefässe von entscheidender Bedeutung. Bisher konnte die Anatomie der Herzkranzgefässe am Abgang aus der Aortenwurzel nur post mortem bestimmt werden, ohne dabei den in vivo existierenden Blutdruck eines lebenden Menschen berücksichtigen zu können. Der Vergleich mit Hilfe der Computertomographie zeigt, dass zwischen anatomischen Messungen am lebenden Menschen und Messungen am obduzierten Herzen signifikante Unterschiede in der rechten Koronararterie vorliegen. Auch die markante Abweichung der genauen Position der Abzweigungen sowohl der rechten als auch der linken Koronararterien verdeutlicht, dass diese anatomischen Unterschiede bei der Entwicklung von neuen Behandlungsmethoden und Implantaten berücksichtigt werden müssen. Ein bezeichnendes Beispiel ist das kürzlich eingeführte Verfahren zum perkutanen Aortenklappenersatz, bei dem es zu Komplikationen durch Verschlüsse der Herzkranzgefässe kommen kann.

Erkrankungen der Aortenwurzel, wie z.B. Aneurysmata oder Dissektionen, insbesondere in der aufsteigenden Aorta und/oder im Sinus Valsalva, können für den Patienten lebensbedrohliche Folgen haben. Inzwischen sind jedoch chirurgische Methoden zur Behandlung entwickelt worden. Mit Hilfe von CT und CFD werden die Strömungsparameter in einer gesunden Aortenwurzel mit denen nach zwei verschiedenen operativen Eingriffen

verglichen: Ersetzen der Aorta mit einer Pseudo-Sinus Prothese in Abgrenzung zur sogenannten Cabrol-Technik. Die Simulationsergebnisse für die Anatomie der Cabrol-Technik zeigen niedrige Blutflüsse in die rechte Koronararterie und korrelieren damit sehr gut mit den Nachuntersuchungen von sieben Patienten, die nach der Operation mit der Cabrol-Technik häufiger Verschlüsse der rechten als der linken Koronararterie aufwiesen. Sowohl aufgrund dieser höheren Verschlussraten und der ungewöhnlichen Strömungen in die Cabrol-Prothese, die die Simulationen zeigen, als auch wegen der unverschlossenen rechten Koronararterien bei Patienten mit Direktverbindung von Herzkranzgefässen und Aorta, ist festzustellen, dass möglichst immer eine direkte Verbindung der Koronararterien mit der Aorta angestrebt werden sollte. Dies sind jedoch vorläufige Ergebnisse, die weiterer Untersuchungen bedürfen.

Die beiden ersten Abzweigungen von der Aorta sind die Herzkranzgefässe, die das Herz selbst mit Blut versorgen. Es ist bekannt, dass hämodynamische Einflussgrössen der Wandschubspannung, wie die mittlere Wandschubspannung, der mittlere Gradient der Wandschubspannung und die oszillierende Schubspannung , Regionen voraussagen können, die anfällig für Wandablagerungen sind und dadurch im weiteren Verlauf eine Arteriosklerose ausbilden können. Diese Blutgefässparameter vor Entstehung der Arteriosklerose werden den tatsächlich vorhandenen Wandablagerungen gegenübergestellt sowie die Sensitivität der Parameter und der positive Vorhersagewert mit Hilfe von CT und CFD verglichen.

Die mittlere Wandschubspannung in der rechten Koronararterie zeigt dabei eine grössere Sensitivität als die oszillierende Schubspannung und einen höheren positiven Vorhersagewert als der mittlere Gradient der Wandschubspannung. Zudem kann die mittlere Wandschubspannung leicht berechnet werden und ist daher am besten für einen möglichen klinischen Einsatz geeignet. Der Zusammenhang zwischen der mittleren Wandschubspannung und möglichen Wandablagerungen ist darüber hinaus in der linken Koronararterie noch ausgeprägter. Dort zeigt die mittlere Wandschubspannung eine grössere Sensitivität als der mittlere Gradient der Wandschubspannung und als die oszillierende Schubspannung, während kein signifikanter Unterschied des positiven Vorhersagewerts zwischen der mittleren Wandschubspannung und der oszillierenden Schubspannung besteht. Die mittlere Wandschubspannung ist daher die geeignete Kennzahl zur Früherkennung von Wandablagerungen in sowohl der rechten als auch der linken Koronararterie.

Contents

Chapter I

Introduction

Diseases of the cardiovascular system are the number one cause of death in most developed nations.[1] With the advent of new imaging modalities and the ever increasing computer processing power, many advances have been made in the past few decades to better understand and treat diseases of the heart and cardiovascular system. In this work, we use the tools of computed tomography (CT) and computation fluid dynamics (CFD) to provide information on the anatomy of the aortic root (chapter 2), insights into current treatments of these tissues for aneurysm and dissection of the ascending aorta (chapter 3), and finally a detailed analysis of the ability of the hemodynamic parameters of wall shear stress to accurately predict the future location of plaque development in both the right (chapter 4) and left (chapter 5) coronary artery trees.

We begin with a description of the anatomy of the aortic root, heart, cardiac valves, coronary arteries and an important component of this region - the sinuses of Valsalva. A brief description is also given of two diseases pertinent to this work – those of aneurysm/dissection of the ascending aorta and of atherosclerosis associated with the coronary arteries. We conclude this chapter with a brief description of the main topics and findings of the subsequent chapters.

1.1 The Aortic Root

Throughout evolution, organisms have evolved specialized mechanisms in order to adapt to their environments. The human heart is an example of such a specialization. It appears that each tissue of the heart is precisely positioned within the organ, playing an intricate part in the function of the organ system as a whole.

Some of the most interesting tissue involved with the opening and closing of the leaflets of the heart are those that compose the tissue of the aortic root. Of particular interest are the three pouch-like structures called the Sinuses of Valsalva. These sinuses are not only greatly important in the functioning of the aortic valve,[2-4] but a case can be made for their significance to each cell of the body, because from these tissues form the arteries that feed the heart itself. Without an adequate supply of oxygen and nutrients the heart can no longer function properly, and hence no cell in the body will receive its needed nutrients.

1.2 The Heart

Inferior to the aortic root we find the driving force behind the circulatory system, the heart. It is actually two different pumps combined together in four chambers (two upper level atria and two lower level ventricles). Four valves (tricuspid, pulmonary, mitral, and aortic) between these chambers prevent backflow from the previous chamber. The low-pressure atria are the "waiting rooms" of the heart, while the high-pressure ventricles actually push the blood through the body. Separating the right and left sides of the heart is the septum.

Deoxygenated blood returns through the superior and inferior vena cava, from the rest of the body, and fills the right atrium. It is then held here until the tricuspid valve opens causing the blood to flow into the right ventricle. Once the right ventricle is full, the tricuspid valve closes and the ventricle contracts, expelling the blood through the pulmonary artery to the lungs. The blood picks up oxygen and dispels carbon dioxide, then returns via the pulmonary veins to the left atrium. The mitral valve is opened and blood flows into the left ventricle. Upon contraction of the left ventricle, the aortic valve is opened and blood flows to the rest of the body through the aorta.

1.3 The Anatomy of the Sinuses of Valsalva

Between the aortic valve and the aorta is a junction characterized by three sinuses which support the semi lunar leaflet attachments of the aortic valve. Two of the sinuses connect to the coronary arteries and are opposite the main pulmonary artery - termed the "facing" sinuses. The third sinus (non-coronary) is termed the non-facing sinus. The sinus that gives rise to the right coronary artery is referred to as the right-facing coronary sinus, and the sinus giving rise to the left coronary sinus is referred to as the left facing sinus.

The sinuses between the left ventricle and the aorta are larger than those found between the right ventricle and pulmonary valve.[5] The sinuses are of an ellipsoidal shape and are composed of elastic tissue, which aids in the closer of the valves. In his book, The Aortic Valve, Thrubrikar[6] provides data of the measurements of the sinuses of the aortic valve. The height of the sinuses (hs) was measured to be 19.9 – 24.6 mm (hs = 1.76 x the radius of the base of the ring (Rb), with the mean Rb = 11.3 – 14 mm). The distance the sinuses extend out from the normal lumen of the aortic valve ring can be measured by the total sinuses depth (ds) minus (Rb), namely 5.2 – 6.4 mm (ds – Rb; with ds = 1.46 x Rb = 16.5 to 20.4). These results show a difference of diameter of the lumen of the valve as compare to the total distance of the diameter of the sinuses to be approximately 150%.

FIG. 281.—Plan of the branches.
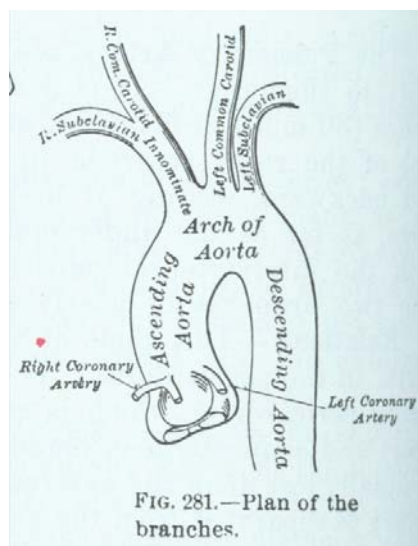
Figure 1-1: Sinuses continuing on to Aortic Arch; note the attachment of the coronary arteries in the upper third of the sinuses.
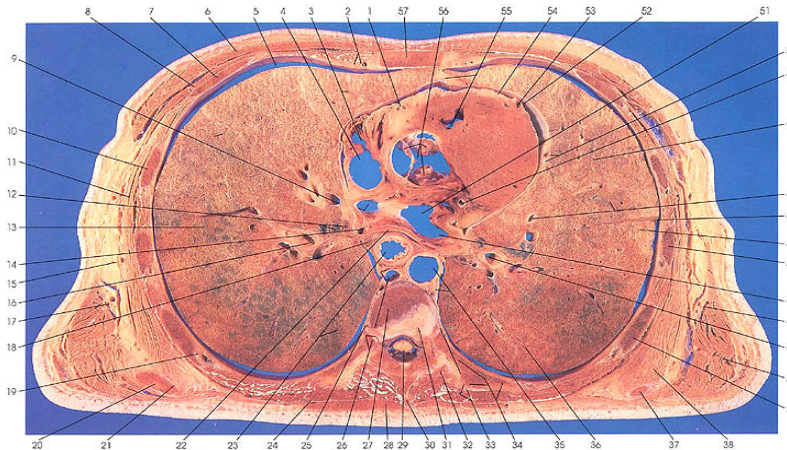
Figure 1-2: *Cross section of chest region. The sinuses of Valsalva can be found at (56).*[7]

1.4 Coronary Arteries

The heart, just as any muscle of the body, must have a constant supply of oxygen and nutrients in order to maintain its continuous function. It does not receive this supply through the blood within its chambers, which it is pumping to the rest of the body, but rather through its own vascularization of the myocardial tissue.

The heart accomplishes this vascularization through the coronary arteries. They originate from the right and left sinuses above the aortic valve, and are usually located in the upper third of the sinuses. They are referred to as the right (Figure 1-3 left) and left main coronary arteries (Figure 1-3 right), respectively.

The right coronary artery passes between the pulmonary artery and the right atrium, and then divides into the transverse, descending, marginal, and infundibular branches.

The left coronary artery is usually larger than the right coronary artery in lumen and is normally 10 – 20 millimeters long.[8] It passes between the pulmonary artery and the left atrium before branching in to the transverse and descending branches.

The branches from the left and right coronary arteries both further branch to smaller vessels and capillaries that supply the cells of the myocardial tissue. After the transfer of oxygen/carbon dioxide and nutrients/wastes in the capillaries, the blood travels through the

4

coronary veins (great cardiac vein, small cardiac vein, middle cardiac vein, posterior vein of the left ventricle, and oblique vein of the left atrium) and drains directly into the right atrium.

In this work, the American Heart Association (AHA) segments[9] (Figure 1-3)[10] will be used to more easily identify the main branches of the right and left coronary arteries. For the right coronary we are interested in segments 1, 2, and 3. For the left coronary we focus on segments 5, 6, 7, 8, 9, 11, and 16.
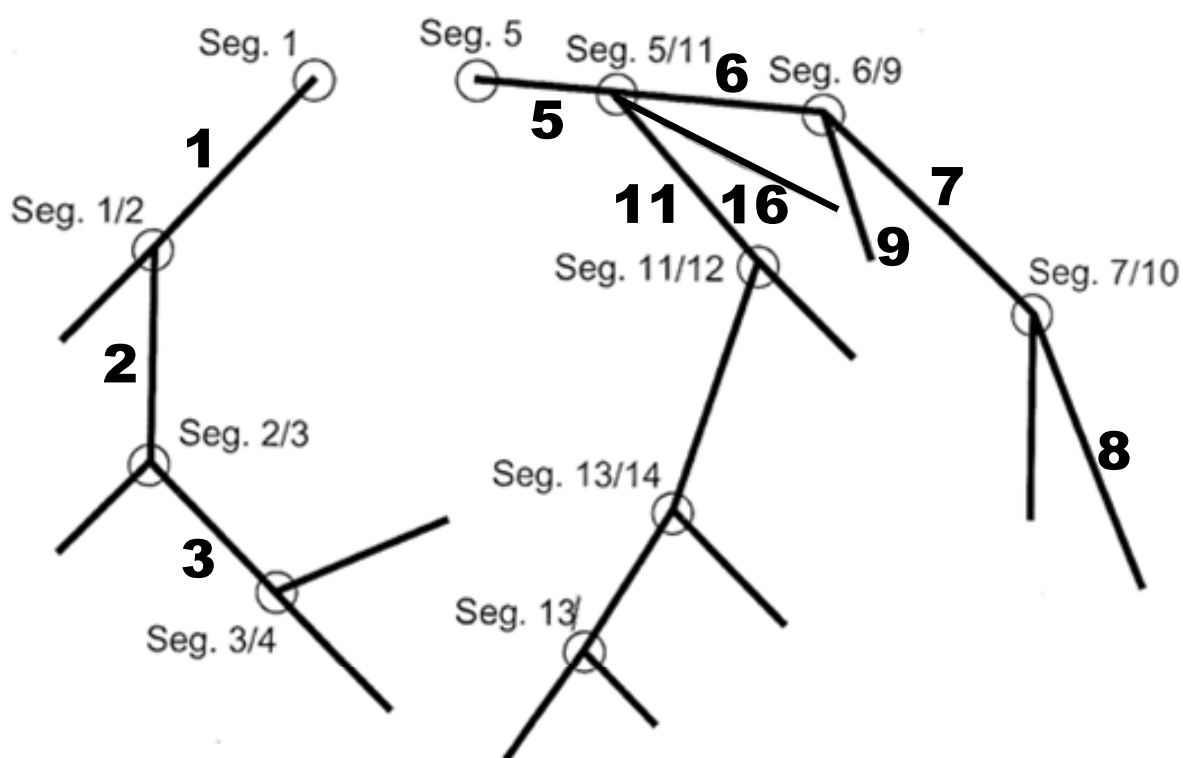
Figure 1-3: *The right coronary tree (left side) and the left coronary tree (right side) with the nomenclature devised by the American Heart Association. The bold numbers (1, 2, and 3 for the right; and 5, 6, 7, 8, 9, 11, and 16 for the left) are the branches studied in this work.[11]*

1.5 Distribution of the Coronaries & Their Attachment to the Sinuses

Extensive variation can be found in the coronary arterial distribution to the myocardial tissue. However the major branches of the network of the coronary arteries are necessarily present. The variation in these major branches is well documented in any standard medical anatomy text or dissector.

For example, Moore's Clinically Oriented Anatomy[11] describes them as follows:

*"Variations in the branching patterns of the coronary arteries are common. In most people the RCA and LCA share approximately equally in the blood supply to the heart. In approximately **15%** of hearts the LCA is dominant in that the posterior interventricular branch is a branch of the circumflex artery. A few people have only a single coronary artery. In other people the circumflex branch arises from the right aortic sinus. Approximately **4%** of people have an accessory coronary artery."*

Grant's Dissector[12] advises to:

*"Expect to find variations of the coronary arteries and their branching patterns. These are common. In about **75%** of the cases, the right coronary artery is dominant… In about **10%** of the cases, the circumflex branch of the left coronary artery, in addition to supplying all of the left ventricle, may send branches to the posterior portion of the interventricular septum and the right ventricular wall. In the remaining **15%**, the posterior portion of the interventricular septum is supplied by both."*

The locations of the origin of the coronary arteries to the sinuses of Valsalva are also associated with much variation. Most texts acknowledge the widespread variation in the ostial location, but give little quantitative reference to this variation. The ostial locations of the coronaries are described more vaguely.

For example, Gray's Anatomy states that:

"*The only branches of the ascending aorta are the two coronary arteries which supply the heart; they arise **near the commencement of the aorta immediately above** the attached margins of the semilunar valves*"

In Cardiac Surgery in the Adult[8]:

"*The right and left coronary arteries originate behind their respective aortic valvar leaflets. The orifices usually are located in the **upper third** of the sinuses of Valsalva, although individual hearts may vary markedly. Because of the oblique plane of the aortic valve, the orifice of the left coronary artery is **superior** and **posterior** to that of the right coronary artery.*"

Moore's Clinically Oriented Anatomy[11]:

"*The right and left coronary arteries arise from the corresponding aortic sinuses at the **proximal part** of the ascending aorta*"

Grant's Atlas of Anatomy: Grant's Dissector[12]:

"*Find the origin and orifice of the left coronary artery **just superior** to the left aortic cusp…Identify the opening of the right coronary artery **just superior** to the right aortic valvule.*"

This lack of a readily available distribution of the normal attachment site of the coronaries to the sinuses of Valsalva is addressed in chapter two, were we provide details of such distributions in a sample of 75 cadavers and 150 patients having undergone computed tomography (CT) examinations.

1.6 Diseases of Interest

Two main diseases will be addressed in this work – 1) dissection and aneurysm of the ascending aorta and/or sinuses of Valsalva and 2) atherosclerosis.

1.6.1 Dissections and Aneurysms

The rapid ejection of blood from the heart and through the aortic valve sends a fast moving pulse through the sinuses of Valsava and the ascending aorta. The blood that comes in contact with the walls of these tissues produces a corresponding force on the walls of the vessel.

Those not completely understood, one theory says that in the case where this shearing causes a disconnecting of the layers of the vessel wall, a dissection occurs. This dissection may or may not be associated with a false lumen, or an opening on the inner most layer of the vessel wall allowing for blood flow to occur inside the lumen created between the two sheared layers.

On the other hand, the forces of blood flow can cause an aneurysm. Though the exact causes of these aneurysms are not fully understood, it is generally accepted that the forces caused by pressure and blood flow stretch the tissue of the vessels, particularly the inner media layer, damaging the vessel and causing it to expand in a radial fashion. If this expansion continues, the patient runs the risk of rupture of the aneurysm which can have a catastrophic outcome if surgical intervention is not immediately performed.

Surgical treatment of both dissections and aneurysms of the ascending aorta are often similar. In its most simple form, during the procedure the diseased tissue (dissected or aneurismal) is excised with temporary detachment of the coronary arteries, an artificial ascending aortic replacement graft is put into place, and the coronary arteries are reattached to the artificial graft. More detail of such procedures is given in chapter three.

1.6.2 Atherosclerosis

Atherosclerosis is a disease in which substances such as cholesterol and calcium accumulate in the vessel walls of arteries, causing a hardening of the vessel, loss of elasticity, and the formation of plaques. It is associated with the major causes of cardiovascular diseases including coronary artery disease, stroke, and heart attack.

Cholesterol is a naturally occurring fat like substance that is produced in the liver, and is essential to the natural functioning of the body. However, too much "bad" cholesterol, or low-density lipoproteins (LDL), and/or not enough "good" cholesterol, or high-density lipoproteins (HDL), can be detrimental to health.

Normal coronary arteries consist of three layers – a smooth inner layer (the tunica intima), a muscular middle layer (the tunica media), and a tough outer layer (the tunica adventitia). Though the exact causes of atherosclerosis are not known, certain risk factors, such as smoking, high blood pressure, high cholesterol, and diabetes can damage the smooth inner lining of the artery. Once this layer is damaged, LDL cholesterol can enter the vessel wall.

Wall shear stress is also known to have an impact on the shape and alignment of the endothelial cells that line the tunica intima. The endothelial cells will align themselves in the direction of flow. Regions of constant flow cause the endothial cells to form an ellipsoid shape and to be tightly pushed together, thus reducing the amount of LDL that enters into the vessel. Regions of slow and oscillatory flow, however, result in cells with polygonal shape and that have no set orientation. This results in an increased uptake of LDL.

The body attempts to defend against this LDL invasion by sending specialized cells, called macrophages, to consume the LDL that enters the vessel wall. These become large cells in the vessel wall called foam cells. The body then attempts to protect the artery against these cells and the fatty streaks within the vessel that they form by surrounding them in a fibrous capsule, which is called a plaque. As the plaque gets bigger, the body attempts to preserve the vessel lumen and corresponding blood flow by allowing the plaque to expand into the elastic tunica media layer. Continued growth of the plaque will lead to obstruction of the vessel lumen, termed a stenosis, which can lead to symptoms such as angina pectoralis.

1.7 Dissertation Outline

The presented work consists of six chapters. We have begun with this first introductory chapter and will now proceed to four journal papers that were completed during the research of the author's Ph.D. studies. Finally, we will conclude with an epilogue of the results of this work and an outlook for future work in this area.

1.7.1 Chapter 2

In chapter two we begin the main text of the work looking at the anatomy of the aortic root, and specifically of the origin of the right and left coronary origins. As all previous studies have reported the distribution of coronary ostial locations only in cadaver hearts, we made measurements in both cadavers (a group of 75) and patients undergoing dual source computer tomography (150 patients) and then compared the two groups. Results from this study not only provide a better basic understanding of the anatomy, but have potential applicability in the treatment of aortic valve disease through percutaneous valve procedures.

1.7.2 Chapter 3

In this chapter we use the tools of computational fluid dynamics (CFD) to explore the changes in fluid flow caused by various surgical procedures to treat diseases of the aortic root, such as aneurysm and dissection, that involve removal of the diseased tissue and implantation of an artificial graft. CFD results of a model representing the normal aortic root anatomy are compared to those of a patient having undergone an ascending aortic replacement with a pseudo-sinus graft and to those of a patient having undergone a unique method of treatment called the Cabrol procedure. Long term clinical and CT imaging follow-up results of seven patients having undergone the Cabrol procedure are also presented.

1.7.3   Chapter 4

This chapter, and chapter five, provides the main work of the dissertation. Chapter four analyses the hemodynamic parameters of average wall shear stress (AWSS), average wall shear stress gradient (AWSSG), oscillatory shear index (OSI), and residency residual time (RRT) with respect to their ability to accurately predict the location of future plaque development. CT data sets of the right coronary artery (RCA) (AHA segments 1, 2, and 3) of 30 patients are used to create geometries for CFD with plaques virtually removed to bring the patient back to a pre-plaque "healthy" state. A CFD analysis is then performed on each of these 30 RCA geometries, with subsequent calculations and comparisons of AWSS, AWSSG, OSI and RRT, with respect to sensitivity and positive predictive value, to the current know plaque locations.

1.7.4   Chapter 5

Chapter five provides a CFD patient study analysis of the left coronary artery, again correlating the hemodynamic wall shear parameters of AWSS, AWSSG, OSI and RRT to plaque locations. Here we explore AHA segments 5, 6, 7, 8, 9, 11 and 16, virtually removing any plaque present, performing the CFD simulations, and then finally correlating AWSS, AWSSG, OSI and RRT wall shear parameters to the current plaque profile of each patient.

1.7.5   Chapter 6

In the closing chapter of this work, we review the results of the undergone studies and present a brief discussion and conclusions. Future potential work is also discussed, as well as a perspective on where the field as a whole may move with future advances.

1.8 References

1   Danaei, G., Ding, E. L., Mozaffarian, D., Taylor, B., Rehm, J., Murray, C. J. and Ezzati, M., The preventable causes of death in the United States: comparative risk assessment of dietary, lifestyle, and metabolic risk factors, PLoS Med, 2009, 6: e1000058.

2   Bellhouse, B. J. and Reid, K. G., Fluid mechanics of the aortic valve, Br Heart J, 1969, 31: 391.

3   Beck, A., Thubrikar, M. J. and Robicsek, F., Stress analysis of the aortic valve with and without the sinuses of valsalva, J Heart Valve Dis, 2001, 10: 1-11.

4   Grande-Allen, K. J., Cochran, R. P., Reinhall, P. G. and Kunzelman, K. S., Finite-element analysis of aortic valve-sparing: influence of graft shape and stiffness, IEEE Trans Biomed Eng, 2001, 48: 647-659.

5   Gray, H., Warwick, R. and Williams, P. L., Gray's anatomy, London], Longman, 1973: xvi, 1471 p.

6   Thubrikar, M., The aortic valve, Boca Raton, Fla., CRC Press, 1990: 221 p.

7   Shier, D., Butler, J. and Lewis, R., Hole's essentials of human anatomy & physiology, Boston, McGraw-Hill Higher Education, 2009: xxvii, 612 p.

8   Cohn, L. H. and Edmunds, L. H., Cardiac surgery in the adult, New York, McGraw-Hill Medical, 2008: xx, 1704 p.

9   Austen, W. G., Edwards, J. E., Frye, R. L., Gensini, G. G., Gott, V. L., Griffith, L. S., McGoon, D. C., Murphy, M. L. and Roe, B. B., A reporting system on patients evaluated for coronary artery disease. Report of the Ad Hoc Committee for Grading of Coronary Artery Disease, Council on Cardiovascular Surgery, American Heart Association, Circulation, 1975, 51: 5-40.

10   Saur, S., Alkadhi, H., Desbiolles, L., Fuchs, T., Székely, G. and Cattin, P., Guided review by frequent itemset mining: additional evidence for plaque detection, International Journal of Computer Assisted Radiology and Surgery, 2009, 4: 263-271.

11   Moore, K. L., Dalley, A. F. and Agur, A. M. R., Clinically oriented anatomy, Philadelphia, Lippincott Williams & Wilkins, 2006: xxxiii, 1209 p.

12	Grant, J. C. B. and Sauerland, E. K., Grant's Dissector, Baltimore, Williams & Wilkins, 1984: xii, 187 p.

CHAPTER II

Ex-Vivo and In-Vivo Coronary Ostial Locations in Humans

Parts of this chapter are published in:

Abstract

Knowledge of the normal in-vivo distribution and variation of coronary ostial locations is essential in the planning of various interventional and surgical procedures. However, all studies to date have reported the distribution of coronary ostia locations only in cadaver hearts. In this study, we sought to assess the distribution of coronary ostial locations in patients using cardiac dual-source computed tomography (CT) and compare these values to those of human cadaveric specimens.

Measurements of the coronary ostia location were performed in 150 patients undergoing dual-source CT and in 75 cadavers using open measurement techniques. All 150 patients had a normal aortic valve function and no previous cardiac intervention or surgery. The location of the right and left coronary origin in relation to the aortic annulus and the height of the sinus of Valsalva were measured.

Mean ostial locations at CT were 17.0 (±3.6)mm and 15.3 (±3.1)mm for the right and left coronary ostia, with large variations of both sides [right: 10.4-28.5mm; left: 9.8-29.3mm]. In cadavers, mean locations were 14.9 (±4.3)mm [5–24mm] for right and 16.0 (±3.6)mm [9–24mm] for left coronary ostia. Comparison of CT and cadaver data showed statistically significant differences for right (P<0.0001) but not left (P=0.1675) coronary ostia.

This study provides data of normal coronary ostial origins and demonstrates significant differences between in-vivo and ex-vivo measurements regarding the right coronary ostium. The observed large variations of coronary ostia origins emphasize the importance of considering such anatomic variations in the development of treatments for diseases of the aortic root.

16

2.2 Introduction

Accurate knowledge of the locations of the coronary ostia in relation to the aortic root is critical for a number of interventional and surgical cardiovascular procedures, including cannulation or catheterization of the coronary arteries, aortic graft repair or root replacement, and implantation of percutaneous aortic valves (PAV) or transapical valve replacement. The recent advent of PAV, providing a non-operative treatment of symptomatic aortic valve disease, has necessitated continuing developments of devices, techniques and treatment protocols for optimization of PAV procedures [14]. With the proximity of the coronary ostia to the aortic annulus and valve leaflets, a particularly challenging issue is the risk of obstruction of the coronary ostia during PAV replacement [2, 4, 9, 11].

In spite of the advances in treatment of aortic valve and root pathology, an in-vivo data set on the variation of the normal coronary ostial location in patients is not available. Though some studies [6, 12, 15, 21, 22] have been performed to determine ostial locations (Table 1-1), each of these studies was limited in that the measurements were taken from cadavers. Further, challenges associated with determining the exact location of the reference points for making such measurements can be seen in the fact that each previous study uses a different method of measurement. Though the ability to make such measurements more precisely using computed tomography (CT) or magnetic resonance imaging (MRI), which allows accurate measurements of three-dimensional cardiac structures, has been foreseen for many years, it was only recently that spatial and temporal resolution was sufficient to do so. Recent developments in CT technology provide a high temporal resolution in combination with an isotropic spatial resolution which allows virtually motion artifact-free imaging of the heart and coronary arteries in any arbitrary three-dimensional plane [16].

In this study we sought to provide data sets representing the normal distribution of the coronary ostial locations relative to the aortic root anatomy in a cohort of consecutive patients undergoing CT imaging of the heart and aortic root. Given the varied methods of measurements of the ostial location of previous ex-vivo studies [6, 12, 15, 21, 22], we also took measurements of the ostial locations in a sample of cadavers to determine the variance of ex-vivo measurements to those taken in-vivo. We sought to identify to what extent the in vivo measurements of the coronary ostial locations differ from those made in cadavers.

Author	#	Sex	Age Range	Ave Age	General	Left (mm)	Right (mm)	Annulus Diameter (mm)
Jantene et al.[12]	100	84% M	9 - 86	30	Measured distance from bottom of the sinus to correpsonding ostium, along the curvature of sinus	13.3	14.8	21.8 (± 3.6)
Cavalcanti et al.[6]	51	-	-	-	*Comissural Line Reference*: 51% below, 34% above, 15% at	12.6 (± 2.61)	13.2 (± 2.64)	-
Vlodaver et al.[22]	55	-	-	-	*Comissural Line Reference*: 40% had 1 or both ostia above	-	-	-
Turner & Navaratnam[21]	38	-	-	-	*Sinotubular Junction Reference*: 84% at or immediately (within 2mm) below	-	-	-
Muriago et al.[15]	23	M & F	29 -79	-	*Sinotubular Junction Reference*: Left (below 69%, above 22%, at 9%); Right (below 78%, above 13%, at 2%)	highest 2mm above junction; lowest 2 mm below	highest 2.5mm above junction; lowest 5 mm below	-

Table 2-1: *Previous Ostial Measurement Studies: Coronary ostial locations in previous ex-vivo studies were measured using multiple reference points. Each is limited by measurements taken solely on cadavers, without re-creation of the natural in vivo environment.*

2.3   Materials and Methods

2.3.1 Cadavers

Seventy-five adult hearts (sex not available) explanted from human cadavers (≥ 40 y/o) were studied by a single observer (J.K.). Right and left coronary ostial locations for each of these hearts were recorded using a standard engineering caliper. In all cadavers, the locations of the coronary ostia were taken as the distance measured orthogonally from the aortic annulus (at the junction of the sinus of Valsalva and the aortic cusps) superior and perpendicular to the center of the coronary ostium (Figure 2-1a). Particular attention was paid to ensure that the lower reference point of the junction of the sinus of Valsalva to the aortic cusp was accurately obtained.

2.3.2 Patients

One-hundred fifty consecutive Caucasian patients (mean age 60.4 ±12.0; range 29-86 years) undergoing cardiac CT from July 2006 to April 2007 were included in this study. Demographic details of the patient population can be found in Table 2. Mean height, weight, and body surface area [8] (BSA) were 169.5 (±9.6) cm, 74.0 (±14.0) kg, and 1.82 (±0.17m2), respectively. There were 58 (38.7%) females (mean age 60.5 ±12.3, range 29–82 years) and 92 (61.3%) males (mean age 60.5 ±11.8, range 33-86 years, P=0.49). BSA for the females was 1.70±0.16m2, while BSA in the male group was 1.93±0.14m2 (P<0.0001 vs. female BSA). The majority of the patients (84%) had a low pre-test likelihood of CAD, whereas an intermediate likelihood was found in 16% of the patients [7]. Indications for cardiac CT were in accordance with recent recommendations [5,10]: atypical chest pain in combination with a low to intermediate risk for coronary artery disease

(n=111), patients prior to extra-cardiac surgery for preoperative evaluation of their coronary arteries (also having a low to intermediate risk for coronary artery

Demographic	Value
Age	60.4 ± 12.0
Gender	61.3% Male
Height	169.5 (±9.6) cm
Weight	74.0 (±14.0) kg
BSA	$1.82(\pm 0.17 m^2$
Pre-test likelihood of CAD	
- Low	84%
- Intermediate	16%

BSA= Body Surface Area, CAD = Coronary Artery Disease

Table 2-2: *Demographic Data: CT patient group demographic information.*

disease, n=16), and patients with acute chest pain and intermediate risk but no electrocardiography changes and no biomarker evidence of an acute coronary syndrome (n=23). Exclusion criteria for CT were: renal dysfunction (serum creatinine level > 1.5mg/dl), known hypersensitivity to iodinated contrast agent, and pregnancy. In addition, patients with cardiac valvular disease (including bicuspid aortic valves), with Marfan or Ehlers-Danlos syndrome, and patients that underwent previous intervention or operation on the heart, thoracic aorta, mediastinum, thoracic cage, and lung were excluded from this study. The institutional review board approved the study; written informed consent was waived since this was a retrospective analysis with no patient identification data included.

2.3.3 CT Data Acquisition

All patients underwent imaging with a dual source CT scanner (Somatom Definition, Siemens Medical Solutions, Forchheim, Germany) for clinical care reasons (i.e., exclusion of coronary artery disease)[1]. Details of scan protocol and data acquisition parameters can be found in [17]. ECG-pulsing for radiation dose reduction was used in all patients [13]. Radiation dose associated with such a CT protocol is approximately 7-9 mSv [18].

2.3.4 CT Data Analysis

All measurements at CT were taken as described above for the cadaveric specimens (Figure 2-1b) using standard cardiac post-processing software (Card IQ, Advantage Workstation 4.0; GE Medical Systems, Milwaukee, Wis, USA). The left coronary ostium (LCO) was located on an oblique coronal multiplanar reconstruction (MPR) which was orientated orthogonally to the plane of aortic annulus. Correspondingly, the localization of the right coronary ostium (RCO) was performed on an oblique sagittal MPR. Measurements were taken from the base of the aortic annulus (at the junction of the sinus of Valsalva and the aortic cusps) to the center of the coronary ostia using an electronic calliper.

The height of the left coronary sinus (LS) was defined as the most distal attachment of the sinus to the aortic root and determined by moving through MPR parallel to the previously used coronal oblique view. Similarly, the height of the right coronary sinus was visualized on parallel sagittal oblique MPR. Again, all height measurements of the sinus were taken orthogonally to the plane of the aortic annulus.

The widths of the aortic root such as the aortic annulus (AA), the sinus of Valsalva (SV), and the sino-tubular junction (STJ) were measured on the same oblique coronal MPR as used for the localization of the left coronary ostium

The inter-observer and intra-observer variation (J.K. and P.S.) was calculated for the first 20 CT data sets for all measured parameters, with a time span of 3 months in between the measurements for both inter- and intra-observer variation. Both intra-observer variation (J.K.) (Right coronary ostium (RCO) = 0.65 ± 1.45mm, left coronary ostium (LCO) = 0.37 ± 1.27mm, annulus diameter (AD) = 1.41 ± 1.22mm, right sinus height (RS) = 0.51 ± 1.14mm, left sinus height (LS) = 0.17 ± 0.97mm), and inter-observer variation (RCO = 0.57 ± 0.92mm, LCO = 0.62 ±
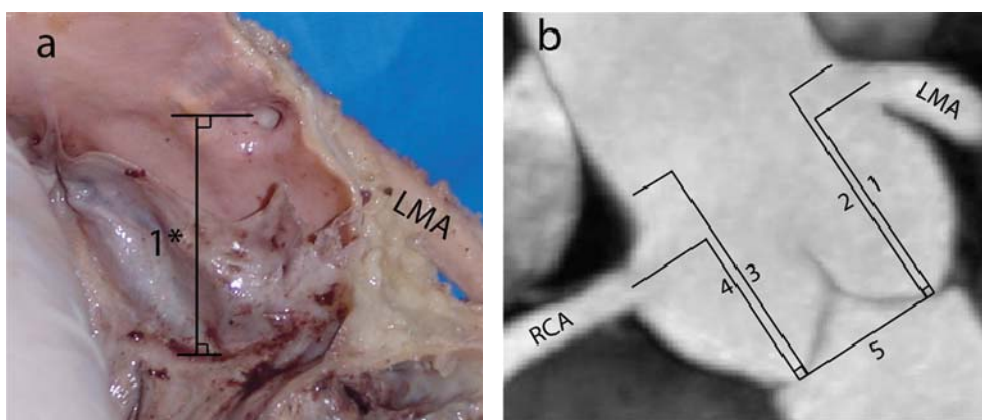
Figure 2-1: *Coronary Ostial and Sinus Measurements – Measurements of the coronary ostial locations in cadavers (a) and with CT (b) were made from the base of the aortic annulus perpendicularly up to the center of the coronary ostium. 1 = Measurement for the left main artery (LMA) ostium in cadavers (a) and in patients with CT (b); 4 = Measurement for the right coronary artery (RCA) ostium with CT. Measurements of the left (2) and right (3) sinus heights were measured by moving through the planes to obtain the attachment of the sinus at the aortic annulus and the sino-tubular junction (yellow dashed line represents the sinus shape through multiple planes). 5 = measurement of the aortic annulus with CT (b).*

0.78mm, AD = 1.46 ± 1.11mm, RS = 0.27 ± 0.9mm, LS = 0.97 ± 1.32mm) were low. Thus, the measurements in the remaining 130 patients were performed by only one reader (J.K.), being the same who made the measurements in the cadaver hearts.

2.3.5 Statistical Analysis

Numerical values were expressed as frequencies or percentages. Age, BMI, BSA, heart rate, ostial locations (i.e., LCO and RCO), sinus heights (i.e., LS and RS), widths of the aortic root (i.e., AA, SW, and STJ), each represented normal distributions for both CT and cadaver measurements as evidenced by Kolmogorov-Smirnov test, and were presented as means ± SD.

Mean differences between the left and right coronary ostium heights as well as sinus heights were assessed using paired t-tests. Differences of CT measures between male and female patients with respect to the LCO, RCO, LS, RS, were
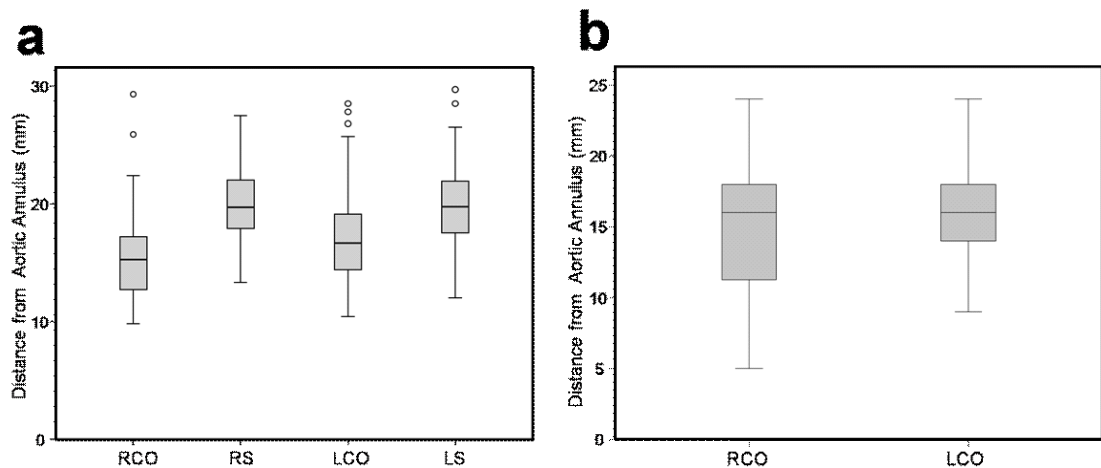
Figure 2-2: *CT Coronary Ostial & Sinus Measurements (a) – Data from CT measurements showing right coronary ostial (RCO) and left coronary ostial (LCO) heights of 17.0 (± 3.6) and 15.3 (± 3.1) mm, respectively. The right (RS) and left (LS) sinus of Valsalva heights had mean values of 19.9 (± 3.2) mm and 19.8 (± 2.7) mm, respectively. Cadaver Coronary Ostial (b) – Data from the cadaver measurements showing right coronary ostial (RCO) and left coronary ostial (LCO) heights of 16.0 (± 3.6) and 14.9 (± 4.3) mm, respectively.*

assessed using unpaired t-tests. Comparisons within the individual groups (CT and cadaver) of the RCO and LCO were performed using paired t-test.

The dependence of measurements on age, BSI, and BMA were investigated using Pearsons correlation. A P value of less than 0.05 was considered significant.

23

Statistical analysis was performed using SPSS software (release 15.0, SPSS Inc., IL, USA).

2.4 Results

The dual-source CT examinations were successfully performed in all 150 patients and no complications occurred. All patients were in a sinus rhythm with a mean heart rate during scanning of 68±11 bpm (range 54–103 bpm). Measurements could be made in all 150 CT data sets and in all 75 human cadaveric specimens.

Table 2-3: *Demographic Data - CT patient group demographic information.*

Hearts	#	Sex	Age Range	Mean Age	General	Right (mm)	Left (mm)	Annulus Diameter (mm)
Cadaver	75	-	-	-	All patients were greater than 40 years of age	14.9 ± 4.3	16.0 ± 3.6	-
CT	150	61% M 39% F	29-86 years	60.4 years	% of left ostium on left sinus 77.0 % of right ostium on right sinus 85.8	Ostium 17.0 ± 3.6 Sinus 19.9 ± 3.2	Ostium 15.3 ± 3.1 Sinus 19.8 ± 2.7	23.0 ± 3.8

2.4.1 Ex-Vivo Cadaver Data

Mean RCO locations in relation to the aortic annulus in the cadaver hearts was 14.9 (±4.3) mm [5–24 mm]. Mean LCO showed a statistically significant difference at 16.0 (±3.6) mm [9–24 mm] (P<0.05).

2.4.2 In-Vivo CT Data

CT data sets of the patients demonstrated a mean location above the aortic annulus of 17.0 (±3.6) mm [10.4-28.5 mm] for the RCO and a mean of 15.3 (±3.1)

mm [9.8-29.3 mm] for the LCO, with significant differences between the two sides (P<0.0001) (Table 2). The mean height of the sinus of Valsalva was 19.9 (±3.2) mm and 19.8 (±2.7) mm for the RS and LS, respectively, with no significant difference between the two sides (P=0.86). The RCO as a percentage of total RS height was 86% (±13) [60-150%] and the RCO as a percentage of total LS height was 77% (±12%) [51-126%] (P<0.0001).

In males, RCO and LCO were located at a mean of 18.0 (±3.7) mm [10.4-28.5 mm] and 15.9 (±3.1) mm [9.9-29.3 mm] above the aortic annulus. In females, RCO and LCO were located at a mean of 15.5 (±2.9) mm [10.9-22.0 mm] and 14.5 (±3.0) mm [9.8-25.9 mm] above the aortic annulus. There were significant differences between the genders for both ostial locations (P<0.0001 for right and P<0.01 for left).

		Male	Female	
RCO	Mean	18.0 (±3.7)	15.5 (±2.9)	P≤0.0001
	Range	10.4-28.5	10.9-22.0	
LCO	Mean	15.9 (±3.1)	14.5 (±3.07)	P≤0.0001
	Range	9.9-29.3	9.8-25.9	
RS	Mean	20.9 (±3.2)	18.3 (±2.6)	P<0.0001
	Range	13.0-29.7	12.0-24.4	
LS	Mean	20.9 (±2.5)	18.2 (±2.2)	P<0.0001
	Range	14.4-27.5	13.3-23.2	
% of RCO on RS	Mean	86.2% (±13.5%)	85.1% (±11.7%)	P=0.61
% of LCO on LS	Mean	75.8% (±10.8%)	79.3% (±12.3%)	P=0.073
Annulus Diameter	Mean	24.0 (±4.2)	21.4 (±2.4)	P<0.0001
	Range	18.1-29.6	16.2-28.1	

Table 2-4: *Comparison of CT measurements by gender - All values are given in mm.*

For males, the mean sinus of Valsalva heights of the RS and LS, respectively, were 20.9 (±3.2) mm [13.0-29.7 mm] and 20.9 (±2.5) mm [14.4-27.5 mm], and 18.3 (±2.6) mm [12.0-24.4 mm] and 18.2 (±2.2) mm [13.3-23.2 mm] for females. There were significant differences between the genders for sinus heights (P<0.0001).

To normalize the ostial locations for male and female, the coronary ostial locations were assessed as a percentage of the total sinus of Valsalva height, the mean RCO and LCO 86.2% (±13.5%) and 75.8% (±10.8%), respectively, for males, and 85.1% (±11.7%) and 79.3% (±12.3%), respectively, for females (P=0.61 for RCO as a percentage of total sinus height; and P=0.073 for LCO as a percentage of total sinus height).

The mean AA diameter was 24.5 (±2.7) mm [18.1-29.6 mm] for males and 21.4 (±2.4) mm [16.2-28.1 mm] for females (P<0.0001).

Figure 2-3: *Coronary Ostial Distribution – Visual representation of the distribution of the locations of the right and left coronary ostia overlaid onto a CT image showing the corresponding anatomy of the aortic root. Note the lower location of the right coronary artery (RCA) ostium and wider variation as compared to the ostium of the left main artery (LMA)*
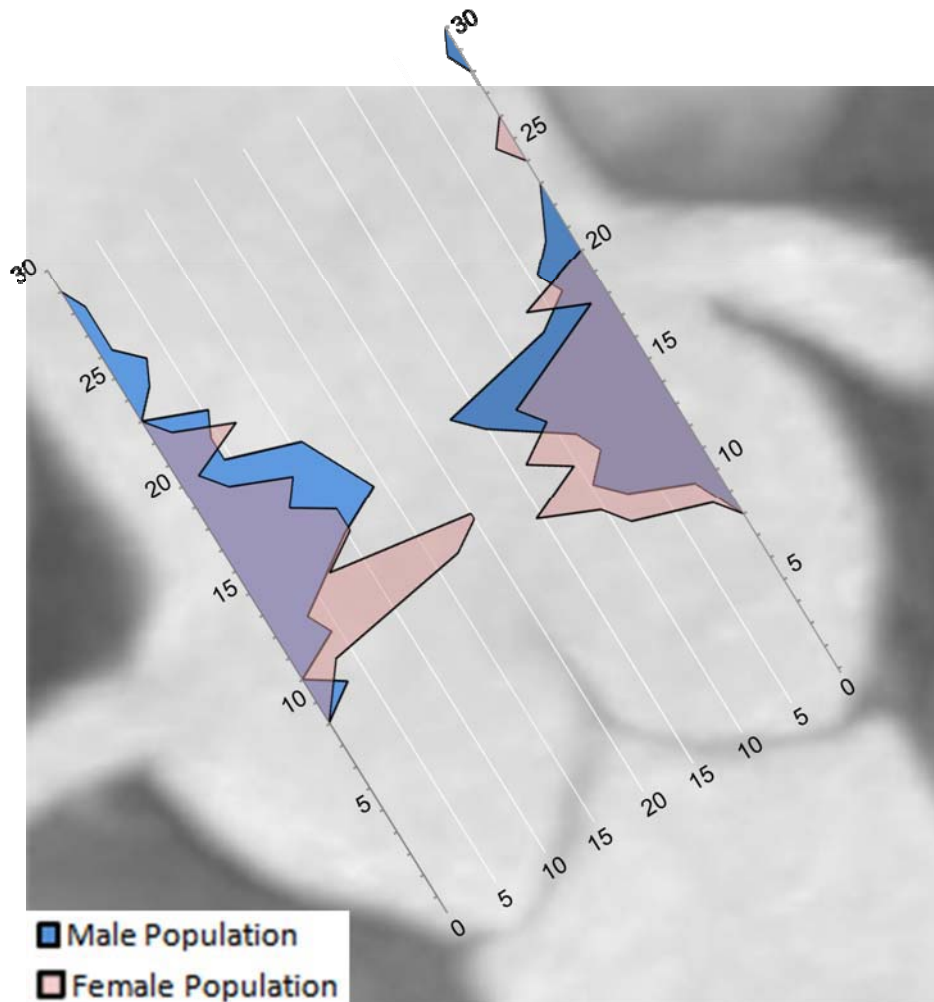
In regards to all measurements (RCO, RS, LCO, LS, AA, SW, STJ), no dependence on age (P>0.05) was found. Similarly, no correlation was found between BMI and RCO or LCO. However, measures of the LS (P<0.01), RS (P<0.05), AA (P<0.05), SW (P<0.05), STJ (P<0.05) did show a significant correlation to BMI. In regards to BSA, a significant correlation (P<0.05) was present for all measurements (RCO, RS, LCO, LS, AA, SW, STJ).

2.4.3 Comparison between in-vivo and ex-vivo data

When comparing the *in-vivo* to the *ex-vivo* measurements, little difference was found in the mean values for the left (CT=15.3 mm, cadaver=16.0 mm) coronary ostium (P=0.1675). A slightly larger, though statistically significant, difference was found for the mean right (CT=17.0 mm, cadaver=14.9 mm) coronary ostium (P<0.0001).

2.5 Discussion

Measurements of cadaveric hearts do not adequately define the coronary ostia in relation to the aortic root in a physiologic, i.e., an *in-vivo,* setting. In this study, we have analyzed the *in-vivo* variation of coronary ostial locations in patients undergoing cardiac CT examinations for a group of standard clinical indications. The right and left ostium tended to be located in the upper portion of the sinus of Valsalva.

Comparison of the CT data with the cadaver heart data revealed significant differences in the location for the right, though not the left, coronary ostia. These differences can be accounted for by: 1) the fundamental differences found in a beating heart under pressure, compared to measurements made on a fixed, non-beating heart (these differences exist in spite of the measurements for the *in-vivo* data being made in diastole, which most closely resembles the *ex-vivo* heart measurement); and, 2) the inherent inaccuracies found in measurements made by hand with a standard engineering caliper, compared to those made using CT – a more precise "electronic caliper". The former point of the high pressure fulfilled diastole aortic sinus is sure to have an impact on the ostial location as compared to the emptied, no pressure cadaveric sinus. The statistically significant differences, found in the *in-vivo* and *ex-vivo* data of this study, as well as the large variations found in both right (10.4-28.5mm) & left (9.8-29.3mm) native ostial locations, are interesting findings that further strengthen the importance for the use of *in-vivo*

measurements, or cadaveric measurement techniques that reproduce the in-vivo environment (for example in the case of the pressurized sinuses of these study, filling the aortic sinus with latex or resin under pressure would likely lower the differences found in the in vivo and ex vivo results) in the development and implementation strategies for devices, techniques, and treatment protocols associated with the aortic root and coronary arteries, as cadaver measurements may not give an accurate representation of the *in-vivo* setting.

2.5.1 Comparison to Previous Studies

Our measurements of left and right sinus of Valsalva height have general agreement with previous studies [3,19, 20].

Because of the various methods of measurements used to assess coronary ostial location in previous cadaveric studies, direct comparisons are challenging. The main points of comparison to the current study are given in Table 1.

Jatene et al. [12] measured the distance from the bottom of the sinus to the corresponding coronary ostium along the surface of the sinus in 100 cadavers. This method should give measurements higher than obtained with the procedure used in our study. However, mean ostial locations of 14.8mm and 13.3mm for right and left coronary origins (standard deviations not given) were found. Our cadaver measurements give slightly higher values for right and left ostial origins, even though we measure a shorter (straighter) distance. Jatene et al. also separated their data into age groups of below and above 40 years of age, which gave different mean ostial locations for the different age groups (<40 y/o; 14.6 mm and 13.0 mm for right and left ostium, respectively, and > 40 y/o; 16.1 mm and 14.9 mm for right and left ostium, respectively). The ostial locations given by Jatene et al. in the over 40-year age group are similar to this study.

Cavalcanti et al. [6] and Vlodaver et al.[22] gave results of their coronary ostial measurements with respect to the intercommissural line (defined in both of their manuscript through a figure as a straight line from the two attachment points of the cusps to the sinus of Valsalva) in cadaveric hearts. It is difficult to compare our

data directly to these studies, as we used the aortic annulus, which correlates to the inferior limit of the sinus, as a reference instead of the intercommissural line.

Two previous studies (by Turner and Navaratnam [21] and Muriago et al. [15]) used the sinotubular junction as the reference for measurements of the coronary ostia. We chose not to re-evaluate the data relative to this position as it is our feeling that the aortic annulus is a more consistent and reproducible reference point, and is more readily viewable using clinical imaging modalities. Further, for insertion of a PAV, the aortic annulus is the hinge point of the over-stented aortic valve and is the more relevant reference in relation to the coronary ostia.

2.5.2 Clinical Implications

Concerning percutaneous and transapical valve replacement, obstruction of the coronary arteries during and/or after implantation remains a risk that can have catastrophic consequences. Boudjemline and P. Bonhoeffer [4] point out that precise placement, with respect to height of the PAV, is crucial. Locations too high above the valve annulus result in coronary ostial obstruction and locations too low can negatively impact left ventricular and/or mitral valve function. The large distribution of ostial locations found in this study, emphasize the importance of considering such variations in the development of treatments.

2.6 Limitations

This study was performed from a patient group consisting of Caucasian male and female patients, and hence does not take into account possible differences in ostial location within different ethnic groups. The study is also limited by inter- and intraobserver variability being performed only for the CT patients group and not for the cadaveric group. Further no data on age or sex was available for the cadaver measurements. Planes used for the measurements made in CT may not be exactly the same as those used in the anatomic specimens.

2.7 Conclusions

This study provides values representing the normal distribution of coronary ostial locations relative to the aortic root in patients and in cadaver specimens. CT showed the right and left ostia to be located in the upper quarter of their respective sinus of Valsalva. The significant differences found between the *in-vivo* and *ex-vivo* data strengthen the call for *in-vivo* measurements, or cadaveric measurement techniques that reproduce the in-vivo environment, to be used in the planning of interventional or surgical devices and procedures involving the coronary ostia. In addition, the large variations found in both right (10.4-28.5mm) & left (9.8-29.3mm) coronary ostial locations are an interesting finding that point to the importance of considering such variations in the development of treatments. Future studies must aim at an assessment of coronary ostial and aortic root anatomy in patients suffering from severe aortic stenosis being candidates to undergo percutaneous or transapical valve replacement.

2.8 References

1. Alkadhi H, Scheffel H, Desbiolles L, Gaemperli O, Stolzmann P, Plass A, Goerres GW, Luescher TF, Genoni M, Marincek B, Kaufmann PA and Leschka S (2008). Dual-source computed tomography coronary angiography: influence of obesity, calcium load, and heart rate on diagnostic accuracy. Eur Heart J 29(6): 766-76.

2. Babaliaros V and Block P (2007). State of the art percutaneous intervention for the treatment of valvular heart disease: a review of the current technologies and ongoing research in the field of percutaneous valve replacement and repair. Cardiology 107(2): 87-96.

3. Berdajs D, Lajos P and Turina M (2002). The anatomy of the aortic root. Cardiovasc Surg 10(4): 320-7.

4. Boudjemline Y and Bonhoeffer P (2002). Steps toward percutaneous aortic valve replacement. Circulation 105(6): 775-8.

5. Budoff MJ, Achenbach S, Blumenthal RS, Carr JJ, Goldin JG, Greenland P, Guerci AD, Lima JA, Rader DJ, Rubin GD, Shaw LJ and Wiegers SE (2006). Assessment of coronary artery disease by cardiac computed tomography: a scientific statement from the American Heart Association Committee on Cardiovascular Imaging and Intervention, Council on Cardiovascular Radiology and Intervention, and Committee on Cardiac Imaging, Council on Clinical Cardiology. Circulation 114(16): 1761-91.

6. Cavalcanti JS, de Melo NC and de Vasconcelos RS (2003). Morphometric and topographic study of coronary ostia. Arq Bras Cardiol 81(4): 359-62, 355-8.

7. Diamond GA and Forrester JS (1979). Analysis of probability as an aid in the clinical diagnosis of coronary-artery disease. N Engl J Med 300(24): 1350-8.

8. Du Bois D and Du Bois EF (1989). A formula to estimate the approximate surface area if height and weight be known. 1916. Nutrition 5(5): 303-11; discussion 312-3.

9. Flecher EM, Curry JW, Joudinaud TM, Kegel CL, Weber PA and Duran CM (2007). Coronary flow obstruction in percutaneous aortic valve replacement. An in vitro study. Eur J Cardiothorac Surg 32(2): 291-4.

10. Hendel RC, Bateman TM, Cerqueira MD, Iskandrian AE, Leppo JA, Blackburn B and Mahmarian JJ (2005). Initial clinical experience with regadenoson, a novel selective A2A agonist for pharmacologic stress single-photon emission computed tomography myocardial perfusion imaging. J Am Coll Cardiol 46(11): 2069-75.

11. Huber CH, Tozzi P, Corno AF, Marty B, Ruchat P, Gersbach P, Nasratulla M and von Segesser LK (2004). Do valved stents compromise coronary flow? Eur J Cardiothorac Surg 25(5): 754-9.

12. Jatene MB, Monteiro R, Guimaraes MH, Veronezi SC, Koike MK, Jatene FB and Jatene AD (1999). Aortic valve assessment. Anatomical study of 100 healthy human hearts. Arq Bras Cardiol 73(1): 75-86.

13. Leschka S, Scheffel H, Desbiolles L, Plass A, Gaemperli O, Valenta I, Husmann L, Flohr TG, Genoni M, Marincek B, Kaufmann PA and Alkadhi H (2007). Image quality and reconstruction intervals of dual-source CT coronary angiography: recommendations for ECG-pulsing windowing. Invest Radiol 42(8): 543-9.

14. Lutter G, Ardehali R, Cremer J and Bonhoeffer P (2004). Percutaneous valve replacement: current state and future prospects. Ann Thorac Surg 78(6): 2199-206.

15. Muriago M, Sheppard MN, Ho SY and Anderson RH (1997). Location of the coronary arterial orifices in the normal heart. Clin Anat 10(5): 297-302.

16. Scheffel H, Alkadhi H, Plass A, Vachenauer R, Desbiolles L, Gaemperli O, Schepis T, Frauenfelder T, Schertler T, Husmann L, Grunenfelder J, Genoni M, Kaufmann PA, Marincek B and Leschka S (2006). Accuracy of dual-source CT coronary angiography: First experience in a high pre-test probability population without heart rate control. Eur Radiol 16(12): 2739-47.

17. Stolzmann P, Scheffel H, Schertler T, Frauenfelder T, Leschka S, Husmann L, Flohr TG, Marincek B, Kaufmann PA and Alkadhi H (2007). Radiation dose estimates in dual-source computed tomography coronary angiography. Eur Radiol.

18. Stolzmann P, Scheffel H, Schertler T, Frauenfelder T, Leschka S, Husmann L, Flohr TG, Marincek B, Kaufmann PA and Alkadhi H (2008). Radiation dose estimates in dual-source computed tomography coronary angiography. Eur Radiol 18(3): 592-9.

19. Swanson M and Clark RE (1974). Dimensions and geometric relationships of the human aortic valve as a function of pressure. Circ Res 35(6): 871-82.

20. Thubrikar M (1990). The Aoric Valve, CRC Press, Inc., Boca Raton, Florida, U.S.A.

21. Turner K and Navaratnam V (1996). The positions of coronary arterial ostia. Clin Anat 9(6): 376-80.

22. Vlodver Z, Vlodaver, Neufeld HN, Edward JE (1975). Coronary Arterial Variations in the Normal Heart and in Congential Heart Disease. New York: Academic Press Inc.

CHAPTER III

Long-Term Follow-up, Computed Tomography and Computational Fluid Dynamics of the Cabrol Procedure

Parts of this chapter were submitted for publication in:

Abstract

The Cabrol procedure is characterized by insertion of an ascending aortic composite graft with reimplantation of the coronary arteries by the interposition of a graft tube. Our purpose is to report the clinical long-term follow-up and computed tomography (CT) findings in patients having undergone the Cabrol procedure and to determine blood flow in the Cabrol graft using computational fluid dynamics (CFD).

Clinical follow-up (76.6±16.6months) and dual-source CT angiography data of 7 patients (all males, mean age 54.9±9.6years) with 12 Cabrol grafts (LMCA, n=7; RCA, n=5) were reviewed. In 2 patients, the RCA was directly reattached to the aortic graft. CFD were calculated using CT data of a patient with the Cabrol procedure and compared to those in a Valsalva graft and a healthy aortic root.

CT showed one occluded (to the LMCA) and one subtotally occluded (to the RCA) Cabrol graft. Six grafts to the LMCA and three to the RCA were fully patent, similar to the two directly reattached RCA. 14% (1/7) of the left and 40% (2/5) of the right Cabrol grafts were occluded. CFD results show similar blood flow parameters into the coronaries for the healthy aortic root and Valsalva graft. In the Cabrol graft, a spiraling flow pattern with low flow into the RCA was found (Systole: RCA=1ml/min; Diastole: RCA=1ml/min).

Our study indicates low flow rates particularly into the right Cabrol graft correlating with a higher incidence of occlusions of the right as compared to the left Cabrol graft at long-term follow-up.

3.2 Introduction

There are currently several techniques available for the surgical replacement of the aortic root. These procedures include a replacement graft for the ascending aorta and can be associated with or without concomitant aortic valve replacement. The replacement graft can be a straight cylindrical type or one with Valsalva shape that more accurately mimics normal aortic root flow for the valve, and into the coronary ostium[1, 2].

The button technique has become the standard method of reattachment of the coronary arteries[3]. For instances in which the button technique is not applicable[4, 5], e.g. during re-operative procedures or in cases where the coronary arteries are challenging to mobilize, the Cabrol procedure can be used[6]. In this now rarely applied procedure, an additional smaller diameter graft (Dacron or polytetrafluoroethylene (PTFE)) is anastomosed side-to-side with the ascending aortic graft and end-to-end to the coronary attachments.

It has previously been shown that the specific technique of coronary re-implantation (Bentall, "button", or Cabrol procedure) is significantly associated with the outcomes of aortic root replacement[5]. However, while Cabrol et al.[7] report a very positive 5 year outcome in 30 patients (20 aneurysm, 10 dissection), Gelsomino et al.[8] advise against the use of the Cabrol procedure based on their 16 year follow-up in 45 patients (17 dissection, 10 annuloaortic ectasia, 5 atherosclerotic aneurysm and 5 poststenotic dilation). It is not known which factors lead to this disparity between the studies. Nevertheless, the consensus today is that the button technique should be used in general, whereas the Cabrol procedure should only be performed when the former is not possible[3, 9-11].

In this study, we report clinical long-term follow-up data and dual-source computed tomography (CT) imaging findings in 7 patients having undergone the Cabrol procedure. In addition, we describe blood flow patterns based on computational fluid dynamics (CFD) calculations using CT datasets of a patient treated with the Cabrol procedure, and compare them with those in a Valsalva graft and a normal healthy aortic

root. Finally, based upon these calculations we provide potential factors to better understand the reported negative outcomes of the Cabrol procedure.

3.3 Materials and Methods

3.3.1 Patient population

Between May 1965 and December 2004, 640 consecutive patients underwent a redo procedure of replacement of the aortic valve or root and/or composite replacement valve. The Cabrol procedure as a coronary connection to the conduit was used in 3.9% (25) of patients undergoing a composite ascending aorta and aortic valve replacement. The indications for using the Cabrol procedure were: general redo procedures, extensive calcification of the aneurysmal aorta, and low coronary ostia. From these 25 patients, 6 were lost for follow-up and 12 died. Thus, we included seven patients (all males, mean age 54.9±9.6 years, range 40-72 years) in our study.

3.3.2 Clinical Follow-up

All clinical data were obtained by retrospective review of medical records. Postoperative follow-up information was obtained by periodical cardiological reports and questionnaires. Cumulative follow-up totalled 44.67 patient years and was 100% complete. Clinical follow-up extended to a maximum of 104 months and the mean follow-up interval was 76.6±16.6 months (median 74 months).

3.3.3 Computed Tomography

All patients underwent imaging with a dual-source CT scanner (Somatom Definition, Siemens Medical Solutions, Forchheim, Germany). Details of scan protocol and data acquisition parameters can be found in[12]. ECG-pulsing for radiation dose reduction was used in all patients[13], leading to an average effective radiation dose of 7-9 mSv[14].

Table 3-1: *Demographic data, underlying disease at the time of the Cabrol procedure, follow-up time interval, and CT imaging findings in the seven patients of this*

Case/age/gender	Underlying disease	Follow-up interval	Cabrol graft	Additional findings
1/42/M	Degenerated homograft with severe aortic regurgitation and periprosthetic aneurysm	7 years and 1 month	Left patent Right occluded	-
2/63/M	Paravalvular regurgitation of mechanical aortic valve	4 years and 10 months	Left graft patent Directly attached RCA patent*	-
3/72/M	Severe aortic regurgitation and ascending aortic aneurysm	5 years and 4 months	Both patent	Subtotally thrombosed periprosthetic aneurysm
4/62/M	Aneurysm of the sinus Valsalva with rupture into the left atrium	8 years and 3 months	Both patent	Fully patent periprosthetic aneurysm
5/56/M	Aortic regurgitation combined with periprosthetic aneurysm	8 years and 8 months	Left patent Right subtotally occluded	Subtotally thrombosed periprosthetic aneurysm
6/49/M	Re-dissection of the aortic root	6 years and 2 months	Left graft occluded Directly attached RCA patent*	-
7/40/M	Marfan syndrome with periprosthetic aneurysm	4 years and 4 months	Both patent	Totally thrombosed periprosthetic aneurysm

study.

M: male. * the right coronary artery was directly attached to the ascending aortic homograft in this patient.

Figure 3-1: *Depiction of the studied geometries from a posterior view: Normal aortic root in (A), pseduosinus (B), and Cabrol (C). During systole, the inlet for the models is the Annulus, and the outlets are the ascending aorta (AscAorta), right coronary artery (RCA), left anterior descending (LAD) coronary and the circumflex (LCX) artery. For the diastolic phase, the inlet for the models is the AscAorta, and the outlets are the RCA, LAD and LCX.*
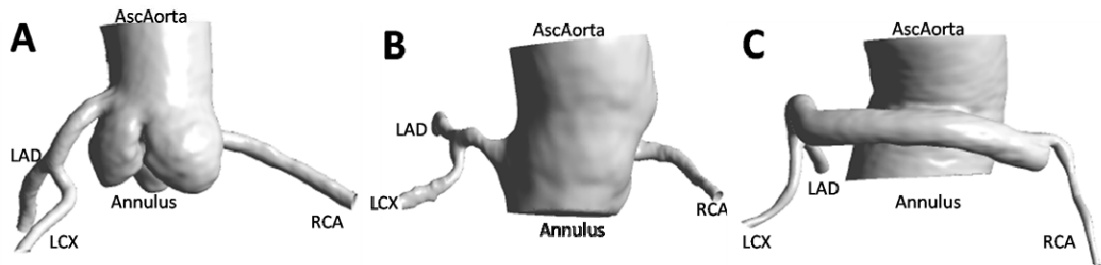
3.4 Computational fluid dynamics

3.4.1 Geometries

Computer models of the geometries of interest were generated by image segmentation of dual-source CT datasets of a normal aortic root, a Valsalva graft, and of a patient having undergone the Cabrol procedure. Each model included the aortic root and proximal part of the ascending aorta, as well as proximal segments of the right (RCA), left anterior descending (LAD) and circumflex (LCX) coronary arteries. Two variations of each model representing maximal flow during the systolic and diastolic phases of the cardiac cycle were used (Figure 3-1).

For the normal aortic root under diastolic conditions, the aortic valve was taken into account in the closed position. The valve was placed in an open position for the systolic phase, thus partially covering the sinus of Valsalva openings.

Models of the two anatomies altered by pseudosinus graft replacement and Cabrol procedure where created in a similar fashion, again including the proximal portions of the right and left coronary arteries, and also the additional graft for the Cabrol procedure.

3.4.2 Boundary Conditions

In order to perform a CFD study, boundary conditions, e.g. prescribed values of velocity or pressure at the inlets and outlets of the respective domain, have to be used. As we are specifically concerned with comparing the effect of changes in geometry of these procedures on the corresponding flow, we developed the strategy below to allow direct comparison of the models.

Steady boundary conditions were used at maximal flow rates of the systolic and diastolic phases of the cardiac cycle in the normal anatomy case. In diastole, an inlet pressure of 110 mmHg was set at the distal end of the ascending aorta geometry. Flow rates where specified at the three outlets (LAD=67 ml/min, LCX=33 ml/min, and RCA=12 ml/min). The pressures at the outlets were then computed and considered to be the natural back pressure of the downstream sections of the coronary arteries and the capillary beds in diastole. These outlet pressures were subsequently used as the coronary artery boundary conditions for the two surgical models in diastole, while the same inlet pressure as in the normal anatomy (110 mmHg) was applied at the distal end of the ascending aorta geometry.

An analogous procedure was used for the systolic boundary conditions. A steady solution at maximal systolic flow in the normal anatomy geometry was first obtained. A flow rate of 5 l/min was set at the aortic annulus. An outlet pressure of 120mmHg was set at the distal end of the ascending aortic geometry. Flow rates where then specified at the three outlets (LAD=33 ml/min, LCX=17 ml/min, and RCA=15 ml/min). The herewith calculated outlet pressures were subsequently used as the coronary artery outlet conditions for the two surgical models.

3.4.3 CFD Settings

Blood was modeled as an non-compressible Newtonian fluid[15] with a density of 1050 kg/m^3 and a viscosity of 0.003 Pascal seconds. An unstructured tetrahedral grid was generated for each model in ICEM-CFD (ANSYS Inc., Pittsburg, PA). Simulations were performed in CFX 11.0 (ANSYS Inc., Pittsburg, PA).

3.5 Results

3.5.1 Clinical and Computed tomography Follow-up

3.5.1.1 Case 1

This 42-year-old man underwent mechanical aortic valve replacement due to anulo-aortic ectasia causing severe aortic regurgitation 15 years ago (Table 3-1). One year later, the patient developed infective endocarditis of the valve prosthesis and was subsequently operated for replacement of the ascending aorta using a homograft along with closure of the paravalvular leak. Over the next 8 years, the homograft progressively degenerated and a periprosthetic aneurysm with severe aortic regurgitation developed. The patient underwent reoperation with replacement of the homograft by a 27 mm aortic valve Composite graft. The Cabrol procedure was performed using a thin-walled, 6 mm PTFE graft. Long-term follow-up CT showed a patent Cabrol graft to the left main artery and an occluded Cabrol graft to the RCA (Figure 3-2). The periprosthetic aneurysm was fully thrombosed. Clinical follow-up at the time of CT showed good general conditions with no clinical or physical limitations (NYHAI).
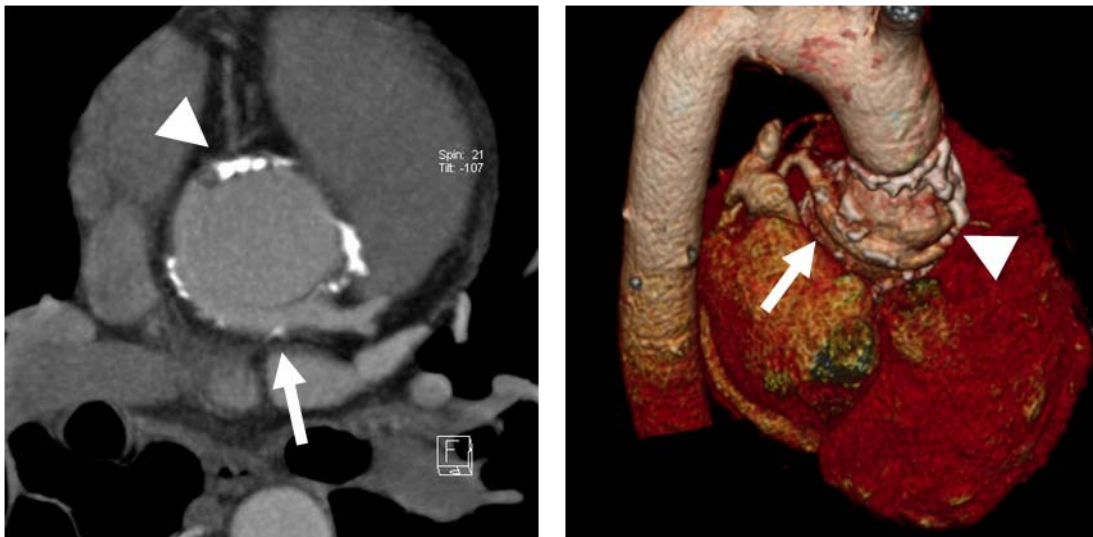
Figure 3-2: *Dual-source CTA in a 42-year-old man performed 7 years and 1 month after the Cabrol procedure. Transverse thin MIP and VR images demonstrate a patent Cabrol graft to the left main artery (arrows) and an occluded Cabrol graft to the right coronary artery (arrowheads).*

3.5.1.2 Case 2

This 63-year-old man underwent biological aortic valve replacement due to severe aortic stenosis 19 years ago (Table 3-1). Because of recurrent degeneration of the valve, the patient was reoperated three times on the valve and aortic root in the subsequent 10 years. Five years ago the patient suffered from hemodynamically significant paravalvular regurgitation. He underwent replacement of the ascending aorta with interposition of a 27 mm Dacron graft combined with a Cabrol procedure. The left main artery was attached to an 8 mm PTFE graft and fixed in an end-to-side fashion to the Dacron graft. The RCA was directly reattached to the Dacron graft without graft interposition. Long-term follow-up CT showed full patency of the Cabrol graft to the left main artery and a patent RCA (Figure 3-3). Clinical follow-up revealed bradyarrhythmia, but no signs of heart failure were found.
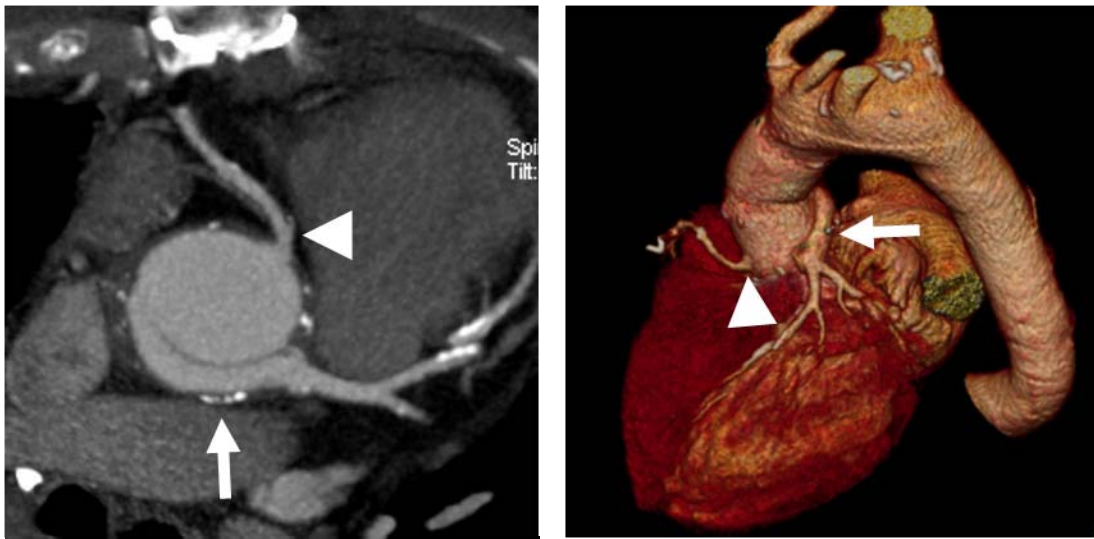
Figure 3-3: *Dual-source CTA in a 63-year-old man performed 4 years and 10 months after the Cabrol procedure. Transverse thin MIP and VR images demonstrate a patent Cabrol graft to the left main artery (arrows) and a patent right coronary artery that was directly reattached to the Dacron graft (arrowheads).*

3.5.1.3 Case 3

This 72-year-old man underwent replacement of the aortic valve due to aortic valve failure after infective endocarditis 21 years ago. After that, a grade III AV block

developed and a DDDR pacemaker was implanted. Sixteen years later the patient suffered from severe aortic regurgitation and an aneurysm of the ascending aorta. The patient underwent replacement of the aortic valve and root by using a 23 mm composite graft. The Cabrol procedure was performed with re-implantation of the coronary arteries by using a 6 mm PTFE graft. Long-term follow-up CT showed a patent Cabrol grafts with only slight wall irregularities. The periprosthetic aneurysm was subtotally thrombosed. Clinical follow-up yielded a good general condition with no discomfort or physical limitations (NYHA I).

3.5.1.4 Case 4

This 62-year-old patient underwent mechanical aortic valve replacement and replacement of the ascending aorta using a supracoronary graft due to a Type A dissection 25 years ago. Twelve years later an aneurysm of the sinus of Valsalva with rupture into the left atrium was detected. The patient underwent replacement of the ascending aorta with a 26 mm Gelweave graft combined with the Cabrol procedure by attaching the native coronary arteries to an 8 mm PTFE graft. The mechanical aortic valve prosthesis was left in place. An additional 6 mm PTFE Cabrol shunt, a small graft that allows drainage of the Cabrol graft, was mounted between the right atrium and the remnant of the native ascending aorta. Long-term follow-up CT revealed a patent periprosthetic aneurysm with the patent Cabrol graft running through the contrast-filled aneurysm. The Cabrol shunt was thrombosed. Clinical follow-up showed fatigue and a reduction of physical performance in everyday life (NYHA II). In addition, the patient reported palpitations at night and recurrent chest pain. No signs of heart failure were found.

3.5.1.5 Case 5

This 56-year-old man underwent replacement of the ascending aorta with a supracoronary graft due to a type-A dissection 10 years ago. Two years later, aortic regurgitation and a periprosthetic aneurysm were diagnosed. The patient was re-operated with replacement of the aortic valve and ascending aorta with a 25 mm aortic

valve graft. Coronary perfusion was maintained using the Cabrol procedure with a 6 mm PTFE graft. Long-term follow-up CT after 8 years and 8 months showed a patent left Cabrol graft and a subtotally occluded right Cabrol graft. The periprosthetic aneurysm was subtotally thrombosed. Clinical follow-up revealed good general condition with no discomfort or physical limitations (NYHA I).

3.5.1.6 Case 6

This 49-year-old man underwent replacement of the ascending aorta with a supracoronary graft due to a type-A dissection 7 years ago. One year later, he suffered from a re-dissection at the proximal aortic graft anastomosis. The patient underwent reoperation of the supracoronary graft including the aortic root with interposition of a 23 mm aortic valve and a 26 mm Composite graft combined with a Cabrol procedure. The left coronary artery was attached to the composite graft using a 6 mm PTFE graft. The RCA was reattached directly to the composite graft without a graft interposition. Long-term follow-up CT showed a patent RCA while the Cabrol graft to the left coronary artery was occluded. The periprosthetic aneurysm was fully thrombosed. Clinical follow-up yielded good general condition with no discomfort or physical limitations of the patient (NYHA I).

3.5.1.7 Case 7

This 40-year-old patient underwent reoperation of the ascending aorta because of a periprosthetic aneurysm after replacement of the ascending aorta due to a chronic, symptomatic Type-A aortic dissection due to Marfan syndrome 5 years ago. Surgery was performed using an interposition 31 mm Composite graft combined with a Cabrol procedure using an 8 mm PTFE graft. Long-term follow-up CT showed patent Cabrol grafts to the left main and RCA as well as a completely thrombosed periprosthetic aneurysm (Figure 3-4). The periprosthetic aneurysm was fully thrombosed. Clinical follow-up revealed good general condition and no physical limitation (NYHA I).

Figure 3-4: *Dual-source CTA in a 40-year-old man performed 4 years and 4 months after the Cabrol procedure. Transverse and coronal thin MIP and VR images demonstrate a patent Cabrol graft to the left main (white arrows) and right coronary artery (arrowheads) as well as the completely thrombosed periprosthetic aneurysm (black arrows).*

3.6 Computational Fluid Dynamics

Systolic Coronary Flow in ml/min			
	LAD	LCX	RCA	Total
Ascending Aorta	33	17	15	65
Valsalva Graft	24	16	15	55
Cabrol Graft	25	10	1	36
Diastolic Coronary Flow in ml/min			
	LAD	LCX	RCA	Total
Ascending Aorta	67	33	12	112
Valsalva Graft	58	32	8	97
Cabrol Graft	78	30	1	110
Percentage of Total Coronary Flow			
	Systolic	Diastolic	
Ascending Aorta	37%	63%	
Valsalva Graft	36%	64%	
Cabrol Graft	25%	75%	

Table 3-2: *Data for the coronary flow in ml/min for each of the three models (ascending aorta, Valsalva graft, and Cabrol procedure) for both systole and diastole show a similar distribution of flow when comparing the normal anatomy with that of the Valsalva graft, although at a lower magnitude. For the Cabrol procedure a limited flow is seen for the right coronary artery (RCA) during diastole and systole, with a different distribution as compared to the normal anatomy and Valsalva graft model.*

3.6.1 Coronary Flow Rates

Coronary flow rates during systole and diastole for the surgical models were compared to the normal anatomy. The Valsalva graft model shows a similar overall distribution of flow through the coronary arteries as the normal anatomy, although at lesser values (Table 3-2). The Cabrol model gives similar flow rates for the LAD. However, lower values were found for the LCX and significantly lower flow for the RCA.
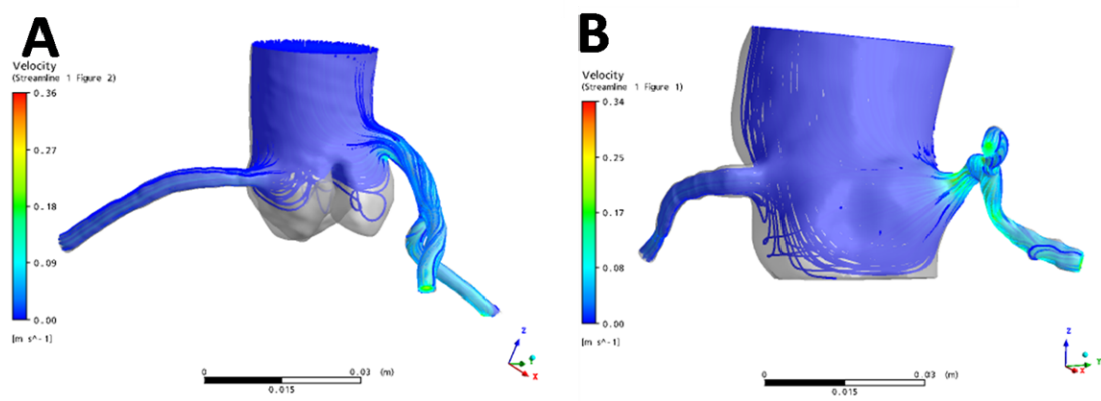
Figure 3-5: *Streamlines of flow for the normal aortic root (A) and Valsalva graft (B) in diastole show similar patterns.*

3.6.2 Flow Characteristics

The flow in the normal aortic root and Valsalva graft models are visualized using streamlines in (Figure 3-5) for both systole and diastole. The flow at the ostium of the two geometries into the coronary arteries is remarkably smooth.

Flow into the Cabrol graft during systole shows a horizontally spiraling, corkscrew-like flow at the opening of the Cabrol graft towards the left coronary connection of the graft. Also present is a vertically spiraling flow just distal to the opening of the Cabrol graft towards the connection to the RCA (Figure 3-6).

A close-up view of the streamlines for the Cabrol graft connection to the native RCA shows that the flow must divert approximately 90° from the inferior end of the Cabrol graft to make its way into the coronary artery.

Figure 3-6: *Streamlines in the Cabrol model showing spiraling flow in both the horizontal and vertical directions in the Cabrol graft (A) and flow into the right coronary (B).*
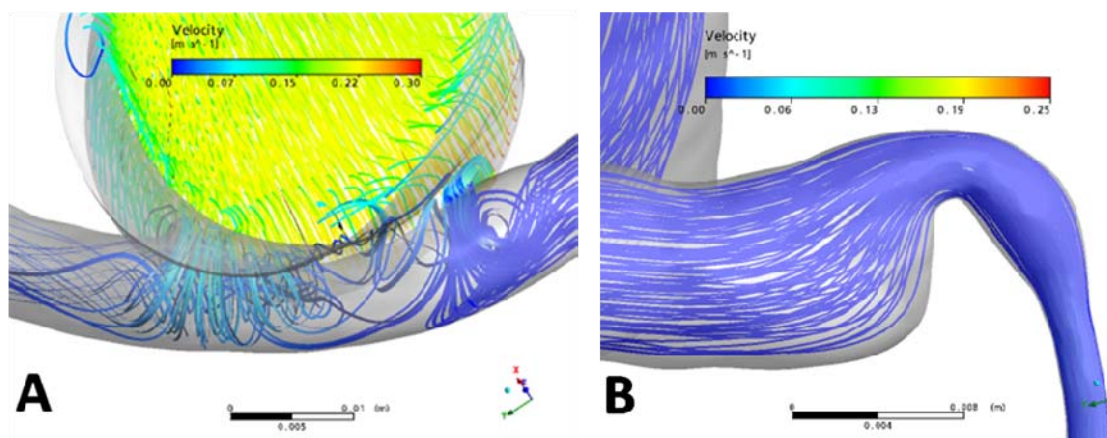
3.7 Comment

The Cabrol procedure provides an accurate, tension-free anastomosis of the native coronary arteries to the Dacron graft that prevents formation of pseudoaneurysms at the coronary ostia[16]. However, it carries the risk for various late complications such as kinking of the Cabrol graft, angulation with occlusion at the coronary artery ostia, and – most importantly - graft occlusion due to thrombosis or stenosis[3, 7]. Therefore, some authors propose its use only in rare instances[3]. Most of the ischemic complications related to the Cabrol procedure described in the literature occurred within 5 years from the initial surgical intervention. These were either due to thrombosis[3] or stenosis of the Cabrol graft[17] at the anastomosis site with the native coronary arteries. In our patient cohort, we found no pseudoaneursyms at the coronary ostia anastomoses, however 14%(1/7) of the left and 40%(2/5) of the right Cabrol grafts were occluded.

Sufficient flow into the coronaries is important for coronary patency and overall cardiac function. The normal aortic root has evolved to provide efficient flow into the coronary ostium, and the results from the CFD study confirm this, while also showing that the Valsalva graft has similar flow characteristics. In both cases, the curved pouch-like structure of the native sinuses of Valsalva (normal aortic root) and the Valsalva graft, respectively, act in such a manner as to more efficiently channel flow to the cardiac tissue.

This contrasts with the Cabrol model, where two specific patterns of the flow are of particular interest: 1)flow into the native RCA from the Cabrol graft, and 2)the spiraling flow formations in the Cabrol graft. The abrupt narrowing of the Cabrol graft as it connects to the RCA has a considerable impact on the resulting flow into the RCA. Although the Cabrol model in this study is only a representation of a single patient having undergone a Cabrol procedure, results found in the CFD study, and in particularly the low flow rates through the right coronary, could partially explain the clinical findings in this (Case 1, 5) and other studies[18] showing occlusion of the right portion of Cabrol grafts.

A unique flow pattern is found in the Cabrol graft itself, especially during systole. The horizontally spiraling flow is produced by the rapid ejection of blood from the heart and past the Cabrol graft. The vertically spiraling flow on the RCA connection side of the Cabrol graft can be accounted for by an attempt of the fluid to equalize the forces (momentum) associated with the flow. These peculiar flows also likely contribute to negative outcomes of the Cabrol graft as shown by the higher rate of RCA closure found in the clinical follow-up of our patients.

3.7.1 Clinical Relevance

While the Cabrol procedure was widely used in the two decades subsequent to its development, Patel et al.[16] state that "the Cabrol procedure is now forgotten by most surgeons and almost unknown by cardiologists". With the known long-term issues of the Cabrol procedure, it is of utmost importance that those who become responsible for follow-up of these patients have knowledge of the particulars of the procedure. There have already been several reported cases of successful follow-up treatments of Cabrol patients made with percutaneous, surgical, as well as combined surgical/endovascular treatments[19], and these types of interventions are likely to become more common as the patients with previous Cabrol procedures age.

In spite of the limited use of the Cabrol procedure, a technique to reattach the coronary arteries during ascending aortic replacement when the button technique is not feasible is still needed. Based on the higher rate of occlusions of the RCA and the

unique flow into the Cabrol graft, together with a patent RCA of all directly attached coronaries, our study suggests the use of a direct connection whenever feasible. These preliminary data warrant further investigation.

3.7.2 Limitations

This study is limited in the analysis of only seven patients for long-term clinical follow-up. The results from the CFD study are limited in the fact that the geometry used was from a single Cabrol procedure.

3.8 Conclusions

Our study provides long term clinical and CT imaging data and demonstrates, for the first time, hemodynamic features of blood flow within the Cabrol graft. Our results from CFD analysis indicate a low and non-laminar flow particularly into the right Cabrol graft correlating well with a higher rate of Graft occlusions when compared with the left Cabrol graft side. Further studies are warranted to directly compare the patency rates of the RCA in the Cabrol procedure to the RCA of directly anastomized coronaries.

3.9 References

1. De Paulis R, Bassano C, Scaffa R, Nardi P, Bertoldo F, Chiariello L. Bentall procedures with a novel valved conduit incorporating "sinuses of Valsalva". Surgical technology international 2004;12:195-200.

2. de Paulis R, Tomai F, Bertoldo F, Ghini AS, Scaffa R, Nardi P, et al. Coronary flow characteristics after a Bentall procedure with or without sinuses of Valsalva. Eur J Cardiothorac Surg 2004 Jul;26(1):66-72.

3. Gelsomino S, Morocutti G, Frassani R, Masullo G, Da Col P, Spedicato L, et al. Long-term results of Bentall composite aortic root replacement for ascending aortic aneurysms and dissections. Chest 2003 Sep;124(3):984-8.

4. Shiono M, Hata M, Sezai A, Iida M, Negishi N, Sezai Y. Reoperation for ascending aortic aneurysm, coronary ostial aneurysm and patent Cabrol trick after bentall operation for aortitis syndrome. Circ J 2005 Jul;69(7):861-4.

5. Bachet J, Termignon JL, Goudot B, Dreyfus G, Piquois A, Brodaty D, et al. Aortic root replacement with a composite graft. Factors influencing immediate and long-term results. Eur J Cardiothorac Surg 1996;10(3):207-13.

6. Cabrol C, Pavie A, Gandjbakhch I, Villemot JP, Guiraudon G, Laughlin L, et al. Complete replacement of the ascending aorta with reimplantation of the coronary arteries: new surgical approach. The Journal of thoracic and cardiovascular surgery 1981 Feb;81(2):309-15.

7. Cabrol C, Pavie A, Mesnildrey P, Gandjbakhch I, Laughlin L, Bors V, et al. Long-term results with total replacement of the ascending aorta and reimplantation of the coronary arteries. The Journal of thoracic and cardiovascular surgery 1986 Jan;91(1):17-25.

8. Gelsomino S, Frassani R, Da Col P, Morocutti G, Masullo G, Spedicato L, et al. A long-term experience with the Cabrol root replacement technique for the management of ascending aortic aneurysms and dissections. The Annals of thoracic surgery 2003 Jan;75(1):126-31.

9. Milano AD, Pratali S, Mecozzi G, Boraschi P, Braccini G, Magagnini E, et al. Fate of coronary ostial anastomoses after the modified Bentall procedure. The Annals of thoracic surgery 2003 Jun;75(6):1797-801; discussion 802.

10. Westaby S, Katsumata T, Vaccari G. Aortic root replacement with coronary button re-implantation: low risk and predictable outcome. Eur J Cardiothorac Surg 2000 Mar;17(3):259-65.

11. Hilgenberg AD, Akins CW, Logan DL, Vlahakes GJ, Buckley MJ, Madsen JC, et al. Composite aortic root replacement with direct coronary artery implantation. The Annals of thoracic surgery 1996 Oct;62(4):1090-5.

12. Alkadhi H, Scheffel H, Desbiolles L, Gaemperli O, Stolzmann P, Plass A, et al. Dual-source computed tomography coronary angiography: influence of obesity, calcium load, and heart rate on diagnostic accuracy. European heart journal 2008 Mar;29(6):766-76.

13. Leschka S, Scheffel H, Desbiolles L, Plass A, Gaemperli O, Valenta I, et al. Image quality and reconstruction intervals of dual-source CT coronary angiography: recommendations for ECG-pulsing windowing. Investigative radiology 2007 Aug;42(8):543-9.

14. Stolzmann P, Scheffel H, Schertler T, Frauenfelder T, Leschka S, Husmann L, et al. Radiation dose estimates in dual-source computed tomography coronary angiography. Eur Radiol 2008 Mar;18(3):592-9.

15. Boutsianis E, Dave H, Frauenfelder T, Poulikakos D, Wildermuth S, Turina M, et al. Computational simulation of intracoronary flow based on real coronary geometry. Eur J Cardiothorac Surg 2004 Aug;26(2):248-56.

16. Patel D, Arteaga RB, Robinson VJ, Patel NA, Kapoor D. Angina, an unusual and late complication of the Cabrol procedure: a case report and review of the literature. The American journal of the medical sciences 2008 Feb;335(2):151-3.

17. Coram R, George Z, Breall JA. Percutaneous intervention through a Cabrol composite graft. Catheter Cardiovasc Interv 2005 Nov;66(3):356-9.

18. Witzenbichler B, Schwimmbeck P, Schultheiss HP. Images in cardiovascular medicine. Myocardial infarction caused by occlusion of Cabrol conduit graft. Circulation 2005 Aug 9;112(6):e79-80.

19. Gorlitzer M, Wislocki W, Meinhart J, Grabenwoger M. Treatment of chronic aortic type A dissection with a new designed hybridprosthesis. Eur J Cardiothorac Surg 2007 Feb;31(2):315-7.

CHAPTER IV

Choosing the Optimal Wall Shear Parameter for the Prediction of Plaque Location – A Patient-Specific Computational Study in Human Right Coronary Arteries

Abstract

Average wall shear stress (AWSS), average wall shear stress gradient (AWSSG) oscillatory shear index (OSI), and residence residual time (RRT) are believed to predict areas vulnerable to plaque formation in the coronary arteries. Our aim was to analyze the correlation of these parameters in patients' vessels before the onset of atherosclerosis to the specific plaque sites thereafter, and to compare the parameters' sensitivity and positive predictive value.

We obtained 30 patient-specific geometries (mean age 67.1 ($\pm$9.2) years, all with stable angina) of the right coronary artery (RCA) using dual-source computed tomography (CT) and virtually removed any plaque present. We then performed computational fluid dynamics (CFD) simulations to calculate the wall shear parameters.

For the 120 total plaques, AWSS had on average a higher sensitivity for the prediction of plaque locations (72%$\pm$25%) than AWSSG (68%$\pm$36%), OSI (60%$\pm$30%, $p<0.05$), and RRT (69%$\pm$59%); while OSI had a higher positive predict value (PPV) (68%$\pm$34%) than AWSS (47%$\pm$27%, $p<0.001$), AWSSG (37%$\pm$23, $p<0.001$), and RRT (59%$\pm$34%). A significant difference was also found between AWSSG and RRT ($p<0.01$) concerning PPV.

OSI and RRT are the optimal parameters when the number of false-positives is to be minimized. However, with its higher sensitivity than OSI and its simple calculation, AWSS appears to be the general parameter of choice to accurately identify the largest number of plaques.

4.2 Introduction

Spatial and temporal variations of arterial endothelial wall shear stress (WSS) influence the location of potential atherosclerotic plaque formation.[1-3] While the correlation between WSS and plaque location is not fully understood, several parameters that are derived from WSS distribution, such as average wall shear stress (AWSS), average wall shear stress gradient (AWSSG) oscillatory shear index (OSI), and residence residual time (RRT) have been identified as possible indicators for atherosclerotic lesion prone sites.[4-6] WSS is the direct result of blood flow and, hence, subject specific variations in arterial anatomy will influence those parameters.[7] Computational fluid dynamics (CFD) has proven to be the method of choice for obtaining accurate readings of flow and WSS distribution in subject specific arterial geometries. However, the process beginning with acquisition of the vessel anatomy using imaging techniques such as computed tomography (CT) to the processing of the CFD results, with numerous steps in between, is complex, costly and time consuming. As a result, previous CFD studies have been limited to a small number of investigated vessel geometries (one to seven) [8-11] or have used an averaged anatomy.[12] Another limitation of previous studies has been that they have sought to correlate subject specific WSS parameters to common plaque locations such as vessel bifurcations, rather than correlating them with actual lesion sites of the respective subject.[13]

We present herein an analysis of the hemodynamic parameters AWSS, AWSSG and OSI obtained through a CFD study on the right coronary arteries of 30 patients with plaques virtually removed to replicate the healthy state of the vessels prior to the onset of atherosclerosis. We correlate these parameters to each patient's specific plaque profile and determine the sensitivity and positive predictive value of each parameter with respect to predicting the particular plaque locations.

4.3 Methods

Our patient population consisted of 80% (24/30) males with an average age and body mass index (BMI) of 67.1±9.2 years [range 47-84] and 26.3±4.3 kg/m² [range 15.6-36.3], respectively. Demographic data and clinical characteristics of the patients are summarized in Table 4-1. All plaques studied were stenotic.

	Total
Number. of patients	30 (100%)
Age (years)	67.1 ± 9.2 (47 - 84)
Male/female ratio	24/6 (80.0% / 20.0%)
Body mass index (kg/m2)	26.3 ± 4.3 (15.6 - 36.3)
Heart rate (bpm)	64.6 ± 13.5 (43 – 91)
Risk Factors	
Smoker	22 (73.3%)
Diabetes	3 (10.0%)
High Serum Cholesterol	13 (43.3%)
Arterial Hypertension	16 (53.3%)
Positive family history	5 (16.7%)
Reasons for referral	
Typical angina	5 (16.7%)
Atypical angina	2 (6.7%)
Non-anginal chest pain	23 (76.7%)

Table 4-1: *Patient demographics and clinical characteristics of the study population.*

4.3.1 CT anatomy acquisition and image processing

For each patient, an initial non-contrast enhanced CT scan was performed for calcium scoring. The patient was then injected with a contrast agent in a right antecubital vein. The application was controlled by bolus-tracking in the ascending aorta. The scanning parameters followed a standard protocol.[14] detector

collimation 32 x 0.6mm, slice acquisition 64 x 0.6mm by means of a z-flying focal spot, gantry rotation time 330ms, pitch of 0.2-0.5 depending on the heart rate (HR), tube current time product 330mAs per rotation, and tube potential 120 kV. Both non-enhanced and contrast-enhanced scans were performed from the level of the tracheal bifurcation to the diaphragm. The non-enhanced scan was reconstructed with a B35f kernel at 70% of the R–R interval using 3.0mm non-overlapping slices. The contrast-enhanced CT angiography data set was reconstructed during mid-diastole at 70% of the R–R interval using a slice thickness of 0.75mm (in plane resolution 0.256mm at 512x512 voxels), a reconstruction increment of 0.5mm, and using the soft-tissue convolution kernel B26f. The retrospective study protocol was approved by the local ethics committee who waived the written informed consent requirement.

The lumen of the right coronary artery (RCA), as well as any calcified plaques present, were automatically segmented with a progressive region growing technique in MeVisLab (MeVis Medical Solutions AG, Bremen, Germany), a development environment for medical image processing.. A surface mesh enveloping the vessel lumen and calcified plaques was defined based on the segmentation. This mesh is regarded to represent the lumen surface of the artery in its healthy state. For the subsequent calculations, the surface mesh was truncated manually to only include the first three segments of the RCA defined according to the classification of the American Heart Association.

4.3.2 Computation of blood flow and wall shear parameters

The geometries of the right coronary arteries were smoothed and computational volume grids consisting of approximately 800,000 tetrahedral elements were generated for all geometries using ANSYS ICEM CFD (ANSYS Inc., Pittsburg, PA). CFD simulations of second order accuracy in space and time were performed using the finite-volume code CFX 11.0 (ANSYS Inc., Pittsburg, PA) to

obtain blood flow and wall shear stress fields. Transient flow replicating systolic and diastolic RCA blood flow,[15] Figure 4-1, was applied to the inlet of the proximal

Figure 4-1: *Blood flow into the right coronary artery during one cardiac cycle used as the inlet boundary condition for the flow computations.*
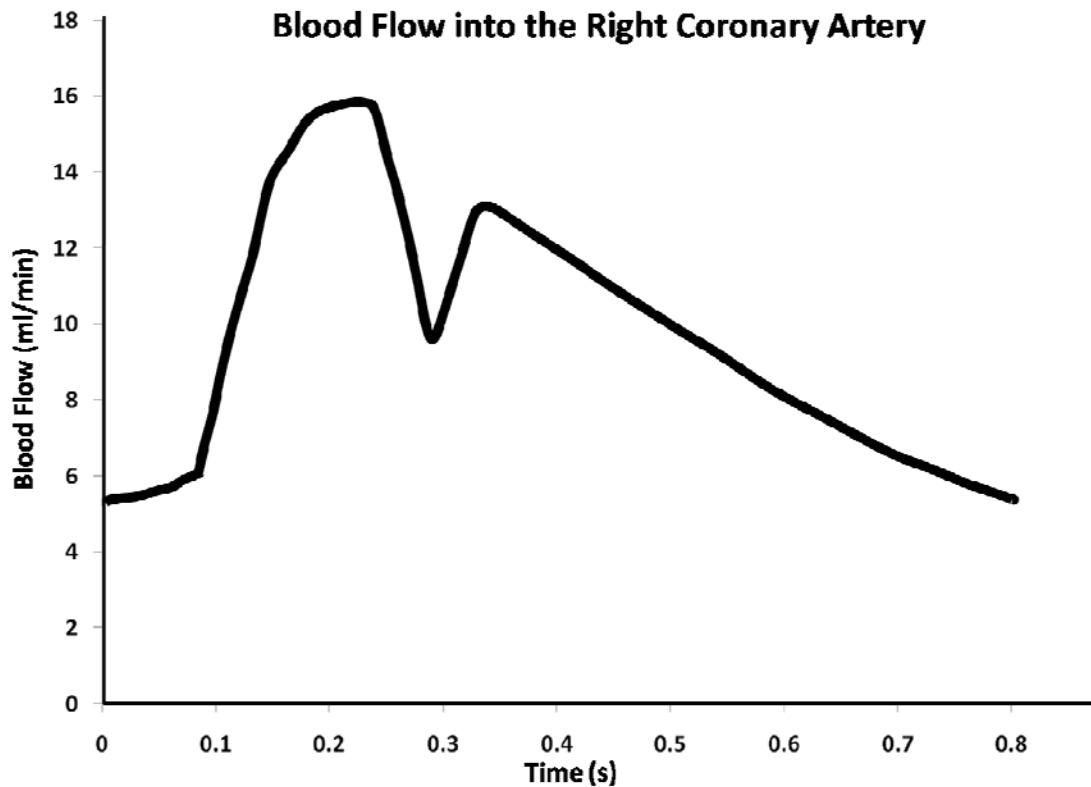
portion of the geometry, corresponding to the part of the RCA just distal to the ostium. Zero pressure was assumed as boundary condition (BC) at the distal outlet of the third AHA segment. No-slip BC was applied at the artery wall. As initial conditions, zero pressure and velocity were prescribed throughout the domain.

Two cardiac cycles were calculated using a time step size of 0.01 seconds, but only the data of the second cycle were evaluated to obtain results independent of the initial conditions. Blood was modeled as an incompressible Newtonian fluid with a density of 1050kg/m3 and a viscosity of 0.0035 Pascal seconds.[16] Grid independence (2.7% - 800k/1.2M cells) as well as cycle (0.08% - 2/3 cycles) and time step size (0.2% - 80/100 time steps) independence tests were performed on a

representative geometry to ensure results independent of the applied temporal and spatial discretization schemes.

AWSS, AWSSG and OSI were derived from the calculated wall shear stress field using MATLAB (The MathWorks Inc., Natick, MA) and Tecplot (Tecplot Inc., Bellevue, WA). These parameters are defined as[1]

$$AWSS = \frac{1}{T}\int_0^T |\vec{\tau}_w| dt \ ,$$

where $|\vec{\tau}_w|$ is the magnitude of the instantaneous wall shear stress vector $\vec{\tau}_w$ and T is the duration of one cardiac cycle,

$$WSSG = \sqrt{\left(\frac{\partial |\vec{\tau}_w|}{\partial x}\right)^2 + \left(\frac{\partial |\vec{\tau}_w|}{\partial y}\right)^2 + \left(\frac{\partial |\vec{\tau}_w|}{\partial z}\right)^2} \quad \text{and}$$

$$AWSSG = \frac{1}{T}\int_0^T (WSSG) dt,$$

where WSSG is the magnitude of the wall shear stress gradient, and $\frac{\partial}{\partial x}$, $\frac{\partial}{\partial y}$ and $\frac{\partial}{\partial z}$ are partial derivates with respect to the x, y and z coordinates, respectively. OSI is defined as,

$$OSI = \frac{1}{2}\left(1 - \frac{\left|\int_0^T \vec{\tau}_w dt\right|}{\int_0^T |\vec{\tau}_w| dt}\right).$$

Finally, RRT is defined as,

$$RRT \sim [(1 - 2 \times OSI) < |\vec{\tau}_w| >]^{-1}.$$

4.3.3 Correlation of wall shear parameters to plaque locations

In order to correlate the three wall shear parameters to each individual patient's plaque distribution, a radiologist first marked the proximal and distal

ends of the plaques in each patient's CT data set and determined the corresponding coordinates. The margins of the plaques where then automatically identified using an intensity-based approach[17] and overlaid onto the transparent rendering of the respective RCA geometry. Most of the automatically obtained plaques corresponded to ones identified by the radiologist. The plaques that were initially not identified by the radiologist (~8%) but designated as such by the algorithm were reassessed and either included in the study as actual plaques or dismissed as artifacts. This hybrid approach was used as the reference standard for plaque identification against which the wall shear stress parameters were subsequently evaluated.

For the comparison of WSS, AWSS and OSI distributions with plaque locations, the RCA geometry was rendered transparently with overlaid plaque margins, and the said wall shear parameters were sequentially projected onto the same transparent RCA surface. In this way, it was possible to determine visually the location of peaks and depressions of the wall shear parameters relative to the reference standard.

We found four basic patterns in which a wall shear parameter correctly identified a plaque, Figure 4-2. These were labeled as proximal (Figure 4-2A – indicative parameter values within the proximal half of the plaque), distal (Figure 4-2B – within the distal half of the plaque), full (Figure 4-2C – within the entire margins of the plaque) and center (Figure 4-2D – focused in the middle region of the plaque). A region indicated by the respective wall shear parameter to be prone to plaque formation, where the reference standard did not identify a plaque, was designated as false-positive. A segment containing three or more false-positives was labeled as a cluster.
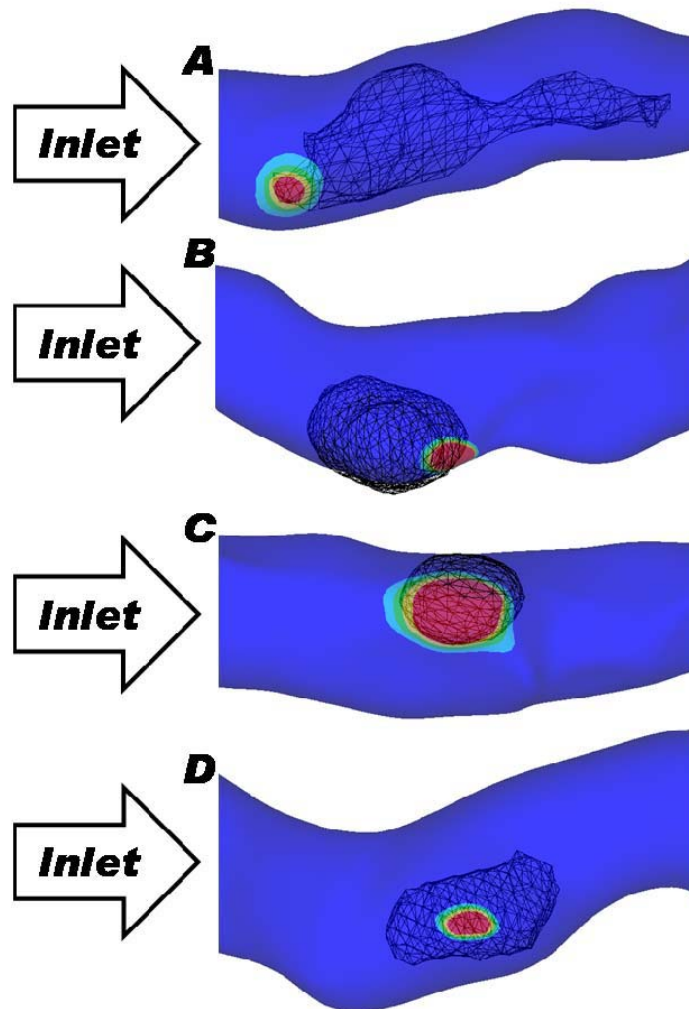
Figure 4-2: *Parameters that correctly identified a plaque were labeled as proximal (A – indicative parameter values within the proximal half of the plaque), distal (B – within the distal half of the plaque), full (C – within the entire margins of the plaque) and center (D – focused in the middle region of the plaque). This figure is for the OSI parameter. Blue represents low OSI values, whereas peak values indicated by red identify a plaque location. The black mesh is a volume representation of the plaque.*

4.3.4 Statistical analysis

All statistical analyses were performed with the software R, release 2.8.1 (www.r-project.org). Quantitative variables are expressed as mean ± standard deviation. Categorical variables are expressed as frequencies or percentages. A

Wilcoxon matched pairs signed rank test was performed to compare the non-Gaussian distributed sensitivity and positive predictive values (PPV) of AWSS, AWSSG, OSI, and RRT. Sensitivity is defined as the number of plaques correctly identified divided by the actual number of plaques (120 for segments 1, 2, and 3). PPV is defined as the number of plaques correctly identified divided by the total number of plaques, both positively and negatively, identified. A p value of < 0.05 is considered statistically significant for all tests.

4.4 RESULTS

In the 30 patients, we found with the reference standard a total of 44, 45 and 31 plaques in segments 1, 2 and 3 of the RCA, respectively. The sensitivity and PPV of correctly identified plaques for the wall shear parameters over the entire RCA are listed in Table 2A. We found AWSS to be significantly more sensitive in predicting plaque locations than OSI ($p < 0.05$, Table 2B). OSI proved to have a significantly higher PPV than AWSS ($p < 0.001$) and AWSSG ($p < 0.001$), as did RRT (AWSS $p < 0.05$ and AWSSG $p < 0.01$).

	AWSS	**AWSSG**	**OSI**	**RRT**
Sensitivity	*72%±25%*	68%±36%	60%±30%	69%±59%
PPV	47%±27%	37%±23%	*68%±34*	59%±34

	Sensitivity p-values			
	AWSS	**AWSSG**	**OSI**	**RRT**
AWSS	-	0.5665	*<0.05*	0.6661
AWSSG	0.1047	-	0.3588	0.8811
OSI	*<0.01*	*<0.001*	-	0.1794
RRT	*<0.05*	*<0.01*	0.2353	-
	PPV p-values			

Table 4- 2: *A) Sensitivity and positive predictive value (PPV) for the prediction of plaque locations in the entire RCA for average wall shear stress (AWSS), average wall shear stress gradient (AWSSG) and oscillatory shear index (OSI). B) p-values when comparing the sensitivities and PPVs for each of the three parameters.*

As shown in Table 3A, the majority of correctly identified plaques were found, for all parameters, in the first and second RCA segments. For the AWSS and RRT parameters, approximately half of the correctly predicted plaques were indicated by low AWSS and high RRT values within the entire margins of the respective plaque as identified by the reference standard (referred to as full parameter location, Figure 2). This was also the case for AWSSG in segment 1, whereas

approximately half of the plaques identified by OSI were located by indicative OSI values in the proximal half of the plaque (proximal parameter location).

For AWSS and AWSSG, each segment showed a large number of false-positive values (Table 3B), including numerous clusters of false-positives. For OSI, a comparably large number of single false-positives, but only one cluster was found in segment 1. RRT had a similar number of single false-positives as OSI, however RRT had more clusters, though not as many as AWSS and AWSSG.

The sensitivity and PPV for each segment are shown in Table 3C. Of the three parameters, AWSS featured the highest sensitivity in segments 1 and 2, while AWSSG was the most sensitive in segment 3. PPV for each segment was <50% for AWSS and AWSSG, but >50% for OSI. PPV for RRT was >50% for all segment 1 and 2, though not segment 3.

Correctly Identified Plaques per Segment & Parameter Location

A

Parameter location	AWSS 1	AWSS 2	AWSS 3	AWSSG 1	AWSSG 2	AWSSG 3	OSI 1	OSI 2	OSI 3	RRT 1	RRT 2	RRT 3	Ref. Std. Seg. 1	Ref. Std. Seg. 2	Ref. Std. Seg. 3
Proximal	7	7	3	3	7	8	13	14	10	7	6	6			
Center	10	11	1	8	4	3	1	6	2	4	0	0			
Full	17	16	9	14	11	7	7	6	5	17	23	7			
Distal	4	3	0	8	6	8	5	3	0	4	3	2			
CIP/Segment	38	37	13	33	28	26	26	29	17	32	32	15	Actual Plaques/Segment 44	45	31
Tot. Correctly Identified	88			87			72			79			Total Actual Plaques 120		

B

Segment	AWSS 1	AWSS 2	AWSS 3	AWSSG 1	AWSSG 2	AWSSG 3	OSI 1	OSI 2	OSI 3	RRT 1	RRT 2	RRT 3
False Positive	15	11	7	14	11	11	16	6	6	9	11	10
Scattered	12	11	6	11	10	9	1	1	1	6	4	4
TOTAL	51	44	25	47	41	38	19	9	9	27	23	22

C — Sensitivity & Positive Predictive Value per Seg

	AWSS 1	AWSS 2	AWSS 3	AWSSG 1	AWSSG 2	AWSSG 3	OSI 1	OSI 2	OSI 3	RRT 1	RRT 2	RRT 3
Sensitivity/Segment	86%	82%	42%	75%	62%	84%	59%	64%	55%	73%	71%	48%
Sensitivity Total	73%			68%			60%			59%		
PPV	43%	46%	34%	41%	41%	34%	58%	76%	65%	54%	58%	34%
PPV Total	42%			36%			66%			59%		

4.5 Discussion

Although it is generally accepted that low AWSS, high AWSSG, high OSI, and high RRT correlate to atherosclerotic lesion prone sites, to our knowledge, the work at hand is the first larger patient study to compare these parameters in patient-specific representations of healthy RCA anatomies to the same patients' detailed plaque profiles once the vessels have become atherosclerotic.

In their review article critically assessing the various arterial transport models, Khakpour et al.[19] describe the prevailing hypotheses that link non-uniform flow as mechanisms for the initiation of abnormal physical and biological events that can lead to atherosclerosis. Four theories are presented – 1) the high shear stress theory which proposes that heightened stresses cause endothelial dysfunction and subsequent local plaque formation; 2) the low shear stress theory argues that the low shear regions that are actually the sites of plaque imitation; 3) oscillatory theory focuses on time dependent factors being the cause; and 4) shear stress gradients make a case for spatial factors being the culprit. The high sensitivity of AWSS found in this study further strengthen the low shear stress theory, while the high PPV of OSI and RRT give clout to the oscillatory theory as contributing factors in the biologic mechanisms for plaque development.

As the majority of plaques identified by the reference standard where found in the first two segments, it is not surprising that this is also where the majority of plaques identified by the wall shear parameters were also located. In general, AWSS and AWSSG identified a larger region of the respective plaque than did OSI or RRT. This can likely be accounted for by the fact that we only investigate the effects of wall shear, without including the numerous other factors important in atherosclerosis such as wall permeability, the layers and thickness of the wall, LDL uptake, recycling of LDL within the walls, etc.

Indicative OSI values were located in almost 50% of the cases in the proximal region of the successfully predicted plaque. As plaque progression has been shown to take place predominantly in proximal to distal direction[21], this suggests that OSI

predicts the actual site of plaque initiation and warrants, together with the high PPV of OSI, further research into this parameter and possible extension thereof with improved sensitivity. In over 50% of cases, RRT values successfully located the full portion of the plaque. Given the high value of PPV for RRT, further research should also be performed on this parameter, again with the possibility of improved sensitivity. The two parameters of OSI and RRT are a better choice for clinical use when the number of false positives is to be minimized. However, when all plaques must be found, with minimal regard to false positive results, then AWSS provides the highest sensitivity.

4.5.1 Limitations

The accuracy of the computed WSS depends on the quality of the employed boundary conditions. As it is not possible to obtain reliable blood flow rates using CT, we used the same pulsatile blood flow for each subject. For the same reason, we assumed a constant RCA outlet pressure, as there are no non-invasive methods for obtaining instantaneous blood pressure levels in the RCA. As a consequence, the performance of the wall shear parameters in terms of sensitivity and PPV is likely to be better than reported here, but it is impossible to say by what margin.

Further assumptions in our model that may affect the WSS distribution are the lack of RCA motion, and the fact that the RCA walls are taken to be rigid. However, it has been shown that the hemodynamic effects of the RCA motion can be ignored as a first approximation.[20] Also, Zeng et al. [21] showed for the right coronary arteries, that wall compliance does not appreciably influence the general flow or WSS patterns.

Finally, a possible concern is the assumption of virtually removing plaque to obtain a representation of the respective RCA in its healthy state. Undoubtedly, vessel remodeling, which we do not account for, will take place as atherosclerosis progresses. However, Achenbach et al. [22] found that stenotic coronary artery

lesions cause negligible remodeling and all plaques found in this study were stenotic.

4.6 Conclusions

We have shown a statistically significant difference between AWSS and OSI in sensitivity and PPV for the identification of atherosclerotic lesion prone sites in the RCA. The higher PPV of OSI and its tendency to pinpoint the precise location of plaque initiation warrant further research. Likewise, further studies should investigate RRT and its higher PPV, yet tendency to locate more of the entire plaque region. The higher sensitivity of AWSS and its simple calculation make it the prime candidate among the three investigated wall shear parameters for potential clinical use.

4.7 REFERENCES

1   Huo, Y., Wischgoll, T. and Kassab, G. S., Flow patterns in three-dimensional porcine epicardial coronary arterial tree, American journal of physiology, 2007, 293: H2959-2970.

2   Zhang, J. M., Chua, L. P., Ghista, D. N., Yu, S. C. and Tan, Y. S., Numerical investigation and identification of susceptible sites of atherosclerotic lesion formation in a complete coronary artery bypass model, Med Biol Eng Comput, 2008.

3   Ku, D. N., Giddens, D. P., Zarins, C. K. and Glagov, S., Pulsatile Flow and Atherosclerosis in the Human Carotid Bifurcation - Positive Correlation between Plaque Location and Low and Oscillating Shear-Stress, Arteriosclerosis, 1985, 5: 293-302.

4   Buchanan, J. R., Jr., Kleinstreuer, C., Truskey, G. A. and Lei, M., Relation between non-uniform hemodynamics and sites of altered permeability and lesion growth at the rabbit aorto-celiac junction, Atherosclerosis, 1999, 143: 27-40.

5   Chatzizisis, Y. S., Jonas, M., Coskun, A. U., Beigel, R., Stone, B. V., Maynard, C., Gerrity, R. G., Daley, W., Rogers, C., Edelman, E. R., Feldman, C. L. and Stone, P. H., Prediction of the localization of high-risk coronary atherosclerotic plaques on the basis of low endothelial shear stress: an intravascular ultrasound and histopathology natural history study, Circulation, 2008, 117: 993-1002.

6   Chatzizisis, Y. S., Coskun, A. U., Jonas, M., Edelman, E. R., Feldman, C. L. and Stone, P. H., Role of endothelial shear stress in the natural history of coronary atherosclerosis and vascular remodeling: molecular, cellular, and vascular behavior, J Am Coll Cardiol, 2007, 49: 2379-2393.

7   Himburg, H. A., Grzybowski, D. M., Hazel, A. L., LaMack, J. A., Li, X. M. and Friedman, M. H., Spatial comparison between wall shear stress measures and porcine arterial endothelial permeability, Am J Physiol Heart Circ Physiol, 2004, 286: H1916-1922.

8   Myers, J. G., Moore, J. A., Ojha, M., Johnston, K. W. and Ethier, C. R., Factors influencing blood flow patterns in the human right coronary artery, Ann Biomed Eng, 2001, 29: 109-120.

9   Berthier, B., Bouzerar, R. and Legallais, C., Blood flow patterns in an anatomically realistic coronary vessel: influence of three different reconstruction methods, J Biomech, 2002, 35: 1347-1356.

10   Wellnhofer, E., Goubergrits, L., Kertzscher, U., Affeld, K. and Fleck, E., Novel non-dimensional approach to comparison of wall shear stress distributions in coronary arteries of different groups of patients, Atherosclerosis, 2008.

11   Stone, P. H., Coskun, A. U., Kinlay, S., Clark, M. E., Sonka, M., Wahle, A., Ilegbusi, O. J., Yeghiazarians, Y., Popma, J. J., Orav, J., Kuntz, R. E. and Feldman, C. L., Effect of endothelial shear stress on the progression of coronary artery disease, vascular remodeling, and in-stent restenosis in humans: in vivo 6-month follow-up study, Circulation, 2003, 108: 438-444.

12   Johnston, B. M. and Johnston, P. R., The relative effects of arterial curvature and lumen diameter on wall shear stress distributions in human right coronary arteries, Phys Med Biol, 2007, 52: 2531-2544.

13   Soulis, J. V., Farmakis, T. M., Giannoglou, G. D. and Louridas, G. E., Wall shear stress in normal left coronary artery tree, J Biomech, 2006, 39: 742-749.

14   Feldman, C. L., Ilegbusi, O. J., Hu, Z., Nesto, R., Waxman, S. and Stone, P. H., Determination of in vivo velocity and endothelial shear stress patterns with phasic flow in human coronary arteries: a methodology to predict progression of coronary atherosclerosis, Am Heart J, 2002, 143: 931-939.

15   Alkadhi, H., Scheffel, H., Desbiolles, L., Gaemperli, O., Stolzmann, P., Plass, A., Goerres, G. W., Luescher, T. F., Genoni, M., Marincek, B., Kaufmann, P. A. and Leschka, S., Dual-source computed tomography coronary angiography: influence of obesity, calcium load, and heart rate on diagnostic accuracy, European heart journal, 2008, 29: 766-776.

16   Berne RM, L. M., Cardiovascular Physiology, St. Louis: CV Mosby, 1986.

17   Milnor, W. R., Hemodynamics, Baltimore, Williams & Wilkins, 1989: 419.

18   Saur, S. C., Alkadhi, H., Desbiolles, L., Szekely, G. and Cattin, P. C., Automatic detection of calcified coronary plaques in computed tomography data sets, Med Image Comput Comput Assist Interv Int Conf Med Image Comput Comput Assist Interv, 2008, 11: 170-177.

19   Khakpour, M. and Vafai, K., Critical assessment of arterial transport models, International Journal of Heat and Mass Transfer, 2008, 51: 807-822.

20   Husmann, L., Leschka, S., Desbiolles, L., Schepis, T., Gaemperli, O., Seifert, B., Cattin, P., Frauenfelder, T., Flohr, T. G., Marincek, B., Kaufmann, P. A. and Alkadhi, H., Coronary artery motion and cardiac phases: dependency on heart rate -- implications for CT image reconstruction, Radiology, 2007, 245: 567-576.

21   Smedby, O., Do plaques grow upstream or downstream? An angiographic study in the femoral artery, Arterioscl Throm Vas, 1997, 17: 912-918.

22   Zeng, D., Ding, Z., Friedman, M. H. and Ethier, C. R., Effects of cardiac motion on right coronary artery hemodynamics, Ann Biomed Eng, 2003, 31: 420-429.

23   Zeng, D. H., Boutsianis, E., Ammann, M., Boomsma, K., Wildermuth, S. and Poulikakos, D., A study on the compliance of a right coronary artery and its impact on wall shear stress, J Biomech Eng-T Asme, 2008, 130: -.

24   Achenbach, S., Ropers, D., Hoffmann, U., MacNeill, B., Baum, U., Pohle, K., Brady, T. J., Pomerantsev, E., Ludwig, J., Flachskampf, F. A., Wicky, S., Jang, I. K. and Daniel, W. G., Assessment of coronary remodeling in stenotic and nonstenotic coronary atherosclerotic lesions by multidetector spiral computed tomography, Journal of the American College of Cardiology, 2004, 43: 842-847.

CHAPTER V

Choosing the Optimal Wall Shear Parameter for the Prediction of Plaque Location – A Patient-Specific Computational Study in Human Left Coronary Arteries

Joseph Knight, MS; Ufuk Olgac, MS; Stefan C. Saur, MS; Dimos Poulikakos, PhD; William Marshall, Jr, MD; Philippe C. Cattin, PhD; Hatem Alkadhi, MD; Vartan Kurtcuoglu, PhD.

5.1 ABSTRACT

We have previously presented results of the ability of average wall shear stress (AWSS), average wall shear stress gradient (AWSSG), oscillatory shear index (OSI), and residence residual time (RRT) to predict areas of plaque formation in the right coronary artery (RCA). Here we provide results of the sensitivity and positive predictive value of these parameters for the left coronary artery (LCA).

We obtained 30 patient-specific geometries (mean age 64.8 ($\pm$10.3) years, all with stable angina) of the LCA using dual-source computed tomography (CT) and virtually removed any plaque present. We then performed computational fluid dynamics (CFD) simulations to calculate the wall shear parameters.

For the 96 total plaques, AWSS had on average a higher sensitivity for the prediction of plaque locations (90%$\pm$22%) than AWSSG (64%$\pm$38%, $p<0.01$), OSI (52%$\pm$34%, $p<0.001$) or RRT (47%$\pm$39, $p<0.001$). RRT had a higher positive predict value (PPV) (48%$\pm$41%) than AWSS (30%$\pm$19%, $p<0.05$), AWSSG (17%$\pm$13, $p<0.001$), or OSI (33%$\pm$25%, $p<0.05$). A significant difference was also found between AWSS/AWSSG ($p<0.001$) and AWSSG/OSI ($p<0.001$) concerning PPV.

AWSS is best suited for potential clinical use in applications that necessitate as many plaques to be identified as possible, regardless of the number of false-positives. RRT is the parameter of choice for clinical applications in which the number of false-positives is to be minimized. Further investigations should focus on a combined parameter that posse's both the high sensitivity of AWSS, while maintaining the high PPV of RRT.

5.2 INTRODUCTION

Hemodynamic parameters of wall shear stress, such as average wall shear stress (AWSS), average wall shear stress gradient (AWSSG), oscillatory shear index (OSI) and residence residual time (RRT) are believed to be possible indicators for atherosclerotic lesion prone sites.[1-3] In a previous study, we gave results for the sensitivity and positive predictive value (PPV) of these four parameters for the right coronary artery (RCA). The relatively simple geometry of the RCA, a minimally curved and non-branching cylinder, provided the platform to develop a method to process and analyze the left coronary artery, a more tortuous and multi-branching vessel.

Herein we present an analysis of the hemodynamic parameters AWSS, AWSSG, OSI and RRT obtained through a CFD study left coronary arteries of 30 patients with plaques virtually removed to replicate the healthy state of the vessels prior to the onset of atherosclerosis. As in our previous RCA study, we again correlate these parameters to each patient's specific plaque profile and determine the sensitivity and positive predictive value of each parameter with respect to predicting the particular plaque locations.

Demographic data and clinical characteristics of the patients are summarized in Table 1. Details of scan protocol and data acquisition parameters for the collection of the geometries of this study can be found in [4]. The retrospective study protocol was approved by the local ethics committee who waived the written informed consent requirement.

Full details of the methods used in this study can be found in the right study. In brief - the lumen of the left coronary artery (LCA), as well as any calcified plaques present, was automatically segmented.[5] For the subsequent calculations, the surface mesh was truncated manually to only include the segments 5, 6, 7, 8, 9, 11, and 16 of the LCA defined according to the classification of the American Heart Association.

Table 5-1: *Patient demographics and clinical characteristics of the study population.*

	Total
Number. of patients	30 (100%)
Age (years)	67.1 ± 9.2 (47 - 84)
Male/female ratio	24/6 (80.0% / 20.0%)
Body mass index (kg/m2)	26.3 ± 4.3 (15.6 - 36.3)
Heart rate (bpm)	64.6 ± 13.5 (43 – 91)
Risk Factors	
Smoker	22 (73.3%)
Diabetes	3 (10.0%)
High Serum Cholesterol	13 (43.3%)
Arterial Hypertension	16 (53.3%)
Positive family history	5 (16.7%)
Reasons for referral	
Typical angina	5 (16.7%)
Atypical angina	2 (6.7%)
Non-anginal chest pain	23 (76.7%)

AWSS, AWSSG, RRT and OSI were derived from the calculated wall shear stress field using MATLAB (The MathWorks Inc., Natick, MA) and Tecplot (Tecplot Inc., Bellevue, WA) as previously defined.

The four wall shear parameters to each individual patient's plaque distribution, a combination of 1) the proximal and distal ends of the plaques in each patient's CT data set were marked by a radiologist and 2) the margins of the plaques where then automatically identified using an intensity-based approach[5] and overlaid onto the transparent rendering of the respective RCA geometry.

We used the nomenclature of four basic patterns developed for the RCA study for identifying when, and to what extent, a wall shear parameter correctly identified a plaque. These were - proximal (indicative parameter values within the proximal half of the plaque), distal (within the distal half of the plaque), full (within the entire margins of the plaque) and center (focused in the middle region of the plaque). A region indicated by the respective wall shear parameter to be prone to plaque formation, where the reference standard did not identify a plaque, was

designated as false-positive. A segment containing three or more false-positives was labeled as a cluster.

All statistical analyses were performed with the software R, release 2.8.1 (www.r-project.org). Quantitative variables are expressed as mean ± standard deviation. Categorical variables are expressed as frequencies or percentages. A Wilcoxon matched pairs signed rank test was performed to compare the non-Gaussian distributed sensitivity and positive predictive values (PPV) of AWSS, AWSSG, OSI, and RRT. A p value of < 0.05 is considered statistically significant for all tests.
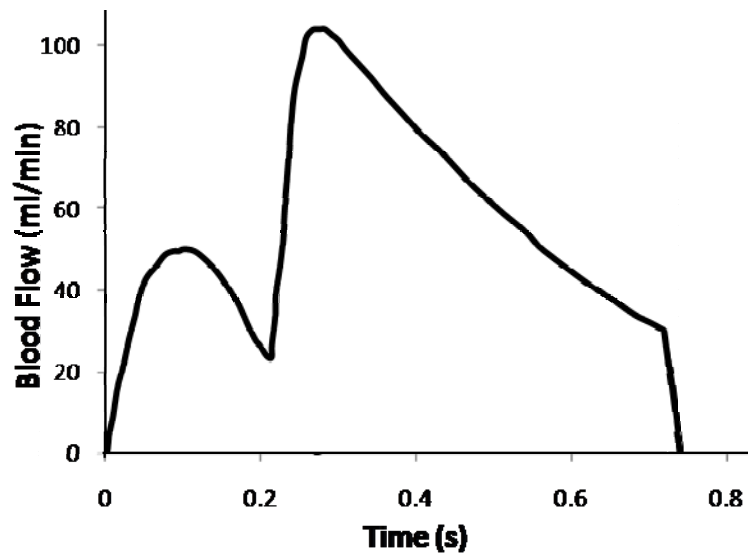
Figure 5-1: *Blood flow into the right coronary artery during one cardiac cycle used as the inlet boundary condition for the flow computations.*

5.3 RESULTS

In the 30 patients, we found with the reference standard a total of 5, 27, 25, 7, 10, 13 and 5 plaques in segments 5, 6, 7, 8, 9, 11 and 16 of the LCA, respectively. Table 2A gives sensitivity and PPV value of correctly identified plaques for the wall shear parameters over the entire LCA. We found AWSS to be significantly more sensitive in predicting plaque locations than AWSSG ($p < 0.001$), OSI ($p < 0.001$) and RRT ($p < 0.001$), Table 2B. AWSS ($p < 0.001$) and OSI ($p < 0.001$) each showed a significantly higher PPV than AWSSG, while RRT had a significantly higher PPV than each of the other three parameters – AWSS ($p < 0.05$), AWSSG ($p < 0.001$) and OSI ($p < 0.05$).

A	AWSS	AWSSG	OSI	RRT
Sensitivity	*90%±22%*	64%±38%	52%±34%	47%±39%
PPV	30%±19%	17%±13%	*33%±25*	48%±41

Sensitivity p-values

B	AWSS	AWSSG	OSI	RRT
AWSS	-	<0.01	*<0.001*	<0.001
AWSSG	<0.001	-	0.2240	0.0815
OSI	*0.3764*	*<0.001*	-	0.2924
RRT	<0.05	*<0.001*	<0.05	-

PPV p-values

Table 2: *A) Sensitivity and positive predictive value (PPV) for the prediction of plaque locations in the entire RCA for average wall shear stress (AWSS), average wall shear stress gradient (AWSSG) and oscillatory shear index (OSI). B) p-values when comparing the sensitivities and PPVs for each of the three parameters.*

As shown in Table 3A, for the AWSS and AWSSG parameter, approximately half of all correctly predicted plaques were indicated by low AWSS values within the entire margins of the respective plaque as identified by the reference standard ("full" parameter location). For OSI and RRT over half of the plaques identified

Table 3: *A) Number of plaques correctly identified by each wall shear parameter per LCA segment and parameter location. B) Number of individual and clustered false-positives for each parameter in each segment. C) Sensitivity and PPV for each parameter in each segment. The sensitivity and PPV totals listed are calculated over the entire LCA and do not represent the averages of the three segment values or averages of the individual sensitivity and PPV values per patient.*

Identified Plaques per Segment & Parameter Location

A

AWSS

Parameter location	Segment 5	6	7	8	9	11	16
Proximal	1	4	5	4	2	4	2
Center	0	3	0	1	1	2	0
Full	3	14	15	2	4	7	1
Distal	0	2	1	0	1	0	0
TOT. Id/Segment	4	23	21	7	8	13	3
Total Identified							**79**

AWSSG

Parameter location	Segment 5	6	7	8	9	11	16
Proximal	1	4	0	0	2	0	0
Center	0	1	2	1	0	1	1
Full	1	10	4	2	1	6	3
Distal	2	5	3	2	0	2	1
TOT. Id/Segment	4	20	9	5	3	8	5
Total Identified							**54**

OSI

Parameter location	Segment 5	6	7	8	9	11	16
Proximal	1	6	7	2	2	3	2
Center	0	0	0	1	0	1	0
Full	1	6	3	1	0	1	0
Distal	0	1	1	0	1	0	0
TOT. Id/Segment	2	13	11	4	3	5	2
Total Identified							**40**

RRT

Parameter location	Segment 5	6	7	8	9	11	16
Proximal	1	7	5	1	2	2	2
Center	0	0	0	0	0	0	0
Full	0	3	3	0	0	0	0
Distal	0	1	1	0	1	1	0
TOT. Id/Segment	1	11	9	1	3	3	2
Total Identified							**30**

Actual Plaques

Segment	5	6	7	8	9	11	16
TOTAL/Segment	5	27	25	7	10	13	5
Total							**92**

B

AWSS

Segment	5	6	7	8	9	11	16
False Positive	26	22	9	5	16	16	4
Clustered	7	6	4	3	2	13	1
TOTAL	47	40	21	14	22	55	7

AWSSG

Segment	5	6	7	8	9	11	16
False Positive	16	11	11	9	13	2	6
Clustered	17	2	3	7	2	23	2
TOTAL	67	17	20	30	19	71	12

OSI

Segment	5	6	7	8	9	11	16
False Positive	21	5	2	1	6	11	3
Clustered	4	0	0	0	0	1	0
TOTAL	33	5	2	1	6	14	3

RRT

Segment	5	6	7	8	9	11	16
False Positive	16	3	1	1	3	11	2
Clustered	0	0	0	0	0	0	0
TOTAL	16	3	1	1	3	11	2

C

Sensitivity & Positive Predictive Value per Segment

AWSS

	5	6	7	8	9	11	16
Sensitivity/Segment	80%	85%	84%	100%	80%	100%	60%
Sensitivity Total							90%
PPV	8%	37%	50%	33%	27%	19%	30%
PPV Total							30%

AWSSG

	5	6	7	8	9	11	16
Sensitivity/Segment	80%	74%	36%	71%	30%	62%	100%
Sensitivity Total							64%
PPV	6%	54%	31%	14%	14%	10%	29%
PPV Total							17%

OSI

	5	6	7	8	9	11	16
Sensitivity/Segment	40%	48%	44%	57%	30%	38%	40%
Sensitivity Total							52%
PPV	6%	72%	85%	80%	33%	26%	40%
PPV Total							33%

RRT

	5	6	7	8	9	11	16
Sensitivity/Segment	20%	41%	36%	14%	30%	23%	40%
Sensitivity Total							47%
PPV	6%	79%	90%	50%	50%	21%	50%
PPV Total							48%

were located by indicative values in the proximal half of the plaque ("proximal" parameter location).

Each of the parameters showed over 50% of the false-positives in segments 5 and 11. AWSS and AWSSG, had particularly high numbers of false-positive values (Table 3B), especially numerous clusters of false-positives. For OSI, a comparably large number of single false-positives, though only a minimal number of clusters were found, and these were concentrated mostly in segments 5 and 11. RRT showed a comparable, though lower, number of false-positives to OSI; however the indicative RRT parameter showed no cluster designations.

The sensitivity and PPV for each segment is displayed in Table 3C. Of the parameters, AWSS featured the highest sensitivity in all segments, except for segment 5 and 16, in which AWSSG had the same and higher values, respectively. The PPV of each segment was <10% for all parameters for segment 5.

5.4 DISCUSSION

In a previous study of "healthy" RCA segments 1, 2 and 3, we provided data correlating the four parameters of AWSS, AWSSG, OSI and RRT to the detailed plaque profiles once the vessels had become atherosclerotic. Here we present a similar analysis for the clinically more relevant, though more complex, geometry of the LCA segments 5, 6, 7, 8, 9, 11 and 16.

Most plaques identified by the reference standard (57% - 52/92) were focused in segments 6 and 7, and hence it is not surprising that these segments generally showed the highest number of accurately predicted plaques for each parameter. However this trend does not transfer over to the sensitivity for each parameter, as each, except for RRT, has the highest sensitivity in a different segment than 6 or 7.

As was the case in the study for the right coronary artery, AWSS and AWSSG had many more false positives and clusters than either OSI or RRT for the LCA. The fewer number of false positives for OSI and RRT can be attributed to the fact that these parameters take into account the time variation of the wall shear more so than the simple averaged values of AWSS and AWSSG. Segment 5, in particular, showed a large number of false positives for all parameters, including OSI and RRT. This can, at least partially, be attributed to the small length of the left main coronary artery before branching into the left anterior descending and circumflex arteries, and the fact that this segment is where the initial pulse of flow is distributed.

In general AWSS and AWSSG identified a larger region of the respective plaque than did OSI or RRT; this was also the case in the RCA. This tendency of AWSS and AWSSG can likely be accounted for by the fact that we only investigate the effects of wall shear, without including the numerous other factors important in atherosclerosis such as wall permeability, the layers and thickness of the wall, LDL uptake, recycling of LDL within the walls, etc.[6] Indicative OSI and RRT values for the LCA were located in almost 50% of the cases in the proximal region of the successfully predicted plaque. As plaque progression has been shown to take place

predominantly in proximal to distal direction[7], this suggests that OSI and RRT may predict the actual site of plaque initiation.

Though there was some variation in the sensitivities of the four parameters, AWSS was found to have a significantly higher sensitivity than the others. Variation in PPV values was also found for the LCA. However, RRT proved to be significantly better than all other parameters. This is an interesting finding as it implies that for those clinical applications in which the largest numbers of plaques need to be found, irrespective of the number of false-positives, AWSS is the parameter of choice. However, for clinical applications when the number of false-positives must be minimized then RRT is the parameter best suited to meet these specifications.

Comparing the overall results of the LCA study presented here to the previous RCA study, we see that all values for sensitivity and PPV were lower for the LCA than for the RCA. The difference in complexity of the two geometries – a simple curved non-branching cylindrical vessel of the RCA as compared to a more tortuous and branching LCA – as well as the different flow profiles throughout the cardiac cycle – a relatively constant flow in the RCA, while a more pronounced pulsatile flow in the LCA – are probable causes of this result. In both the LCA and RCA study, AWSS was found to have the highest sensitivity. Concerning PPV, RRT was clearly the parameter with the highest PPV for the LCA, and though RRT was found to be significantly higher than AWSS and AWSSG, the value of PPV was higher for OSI than RRT, though this was not found to be a statistically significant difference.

The limitations of this study, including those associated with boundary conditions, lack of LCA motion, rigid walls, obtaining the healthy state of the LCA, etc. are each addressed in our initial RCA study. An additional limitation of this study, not found in the RCA study, is that though 30 patients where studied in each, only 92 total plaques were found in the LCA, and these were spread over seven different segments, compared with the 120 plaques spread over 3 segments of the RCA. Inherent challenges associated with obtaining and segmenting LCA geometries that are suitable for CFD are the cause of this limitation, as those

geometries with plaques are more challenging to create an acceptable geometry with proper branching, as compared to the RCA.

5.5 Conclusion

We have shown AWSS to have a significantly higher sensitivity than AWSSG, OSI and RRT for the identification of atherosclerotic lesion prone sites in the LCA, making it the parameter best suited for clinical applications when the largest number of plaques must be identified. When the number of false-positives must be minimized, then RRT, with its significantly higher PPV than the others, is the parameter best suited to for such clinical purposes. Further research into a combined parameter that will allow for both the high sensitivity of AWSS and the highest PPV of RRT should be explored.

5.6 Reference

1   Buchanan, J. R., Jr., Kleinstreuer, C., Truskey, G. A. and Lei, M., Relation between non-uniform hemodynamics and sites of altered permeability and lesion growth at the rabbit aorto-celiac junction, Atherosclerosis, 1999, 143: 27-40.

2   Chatzizisis, Y. S., Jonas, M., Coskun, A. U., Beigel, R., Stone, B. V., Maynard, C., Gerrity, R. G., Daley, W., Rogers, C., Edelman, E. R., Feldman, C. L. and Stone, P. H., Prediction of the localization of high-risk coronary atherosclerotic plaques on the basis of low endothelial shear stress: an intravascular ultrasound and histopathology natural history study, Circulation, 2008, 117: 993-1002.

3   Chatzizisis, Y. S., Coskun, A. U., Jonas, M., Edelman, E. R., Feldman, C. L. and Stone, P. H., Role of endothelial shear stress in the natural history of coronary atherosclerosis and vascular remodeling: molecular, cellular, and vascular behavior, J Am Coll Cardiol, 2007, 49: 2379-2393.

4   Alkadhi, H., Scheffel, H., Desbiolles, L., Gaemperli, O., Stolzmann, P., Plass, A., Goerres, G. W., Luescher, T. F., Genoni, M., Marincek, B., Kaufmann, P. A. and Leschka, S., Dual-source computed tomography coronary angiography: influence of obesity, calcium load, and heart rate on diagnostic accuracy, Eur Heart J, 2008, 29: 766-776.

5   Saur, S. C., Alkadhi, H., Desbiolles, L., Szekely, G. and Cattin, P. C., Automatic detection of calcified coronary plaques in computed tomography data sets, Med Image Comput Comput Assist Interv Int Conf Med Image Comput Comput Assist Interv, 2008, 11: 170-177.

6   Olgac, U., Kurtcuoglu, V., Saur, S. C. and Poulikakos, D., Identification of atherosclerotic lesion-prone sites through patient-specific simulation of low-density lipoprotein accumulation, Med Image Comput Comput Assist Interv Int Conf Med Image Comput Comput Assist Interv, 2008, 11: 774-781.

7   Smedby, O., Do plaques grow upstream or downstream? An angiographic study in the femoral artery, Arterioscl Throm Vas, 1997, 17: 912-918.

CHAPTER VI

Epilogue

6.1. Review of Results

Results from this work focused on providing information to better understand and treat diseases of the aortic root and coronary arteries. A multi-disciplinary approach was taken combining the expertise and tools of three main areas – the radiologist and the tools of computed tomography (CT), the biomedical engineer and the tools of computational fluid dynamics (CFD), and the computer scientist and the tools of parallel processing.

Accurate understanding of the anatomy of interest is of paramount importance for not only CFD results, but also for the development of devices and treatment protocols for clinical purposes. Measurements of cadaveric hearts do not adequately define the coronary ostia in relation to the aortic root in a physiologic, i.e., an in-vivo, setting. Chapter two presents data for the distribution of the coronary ostia in both cadavers and patients having undergone CT. Results showed a statistically significant difference in the right, though not the left, coronary ostia when comparing the ex-vivo cadaver measurements to those of the in-vivo CT. This is important in that all previously obtained measurements to define the anatomy of the coronary ostia were ex-vivo, and not in the under pressure native environment where treatments and devices are to be used. Novel in-vivo treatment protocols of the aortic root, such as percutaneous and transapical aortic valve replacement and their corresponding risk of coronary ostial obstruction, along with the observed large variations of coronary ostia origins found in

this study, emphasize the importance of considering such anatomic variations in the development of treatments.

In chapter three, a CFD analysis is used to compare two different surgical techniques for treatment of aneurysm/dissection of the ascending aorta. Blood flow in a pseudo-sinus graft is compared to that of a patient treated with the Cabrol procedure, and each of these is further compared to a model of the normal healthy aortic root. CFD results showed a similar blood flow into the coronaries for the healthy aortic root and Valsalva graft. In the Cabrol graft, however, a spiraling flow pattern with low flow into the RCA was found. This low flow rate into the right coronary correlated well with clinical and CT follow-up performed on seven patients treated with the Cabrol procedure that showed a higher incidence of right coronary closure than left. Based on the higher rate of occlusions of the RCA and the unique flow into the Cabrol graft, together with a patent RCA of all directly attached coronaries, these results imply that one should use of a direct connection whenever feasible. These preliminary results warrant further investigation.

It is believed that wall shear parameters – such as average wall shear stress (AWSS), average wall shear stress gradient (AWSSG), oscillatory shear index (OSI) and residence residual time (RRT) – can indicate possible atherosclerotic lesion prone sites. However, the ability of each of these hemodynamic parameters to accurately identify specific plaque locations has not been fully investigated in a large patient study. In chapter four and five results are presented for two such patient studies comparing the parameters of AWSS, AWSSG, OSI and RRT in the right (chapter four) and left (chapter five) coronary arteries of 30 patients with plaques virtually removed.

Correlating the results of these wall shear parameters to the patient specific plaque profiles, AWSS was found to have a higher sensitivity than OSI, while OSI and RRT both had a higher positive predict value (PPV) than either AWSS or AWSSG for the right coronary artery. These results point to OSI and RRT being the optimal parameters when the number of false-positives is to be minimized. However, with its higher sensitivity than OSI and its simple calculation, AWSS appears to be the general parameter of choice to accurately identify the largest number of plaques for the right coronary artery.

A similar, though more pronounced correlation was found for the left coronary. AWSS had a higher sensitivity than all three other parameters – AWSSG, OSI, and RRT. For PPV, RRT proved to be significantly higher than all three other parameters, while AWSS and OSI were both significantly higher than AWSSG. These results imply that AWSS is best suited for potential clinical use of the LCA in applications that necessitate as many plaques to be identified as possible, regardless of the number of false-positives. RRT is the parameter of choice for the LCA for clinical applications in which the number of false-positives is to be minimized.

6.2 Future Work

Though much progress has been made in the past decades concerning the use of imaging and computational power to aid in the understanding, diagnoses, and treatment of diseases of the cardiovascular system, the coming decades are likely to see this foundation of research and development pushed more towards actual clinical application. The research presented here is hopefully a small contribution towards the much larger goal of fully automated patient specific analysis of the aortic root and coronary arteries for diagnosis and treatment.

One example of where the future may lead for treatment of diseases of the aortic root, such as those presented in chapter three, would be a system in which a patient is scanned in CT with the aortic root automatically segmented and meshed. Models for different surgical options, for example of various treatment techniques for graft replacements, or locations most suitable for the reattachment of the coronary arteries, could also be created with limited surgical input. These different options would then be run through a CFD analysis with a recommended treatment, along with likely outcomes, given as a final output to further aid the surgeon in providing the best care.

A future example for the coronary arteries and treatment of atherosclerosis might look something like this: an at risk patient for coronary artery disease is scanned to produce models of the coronary tree that are automatically meshed for CFD. The performed CFD analysis shows not only areas of the anatomy at risk for future atherosclerosis initiation, but also provides

possible scenarios for the likely development of future plaque sites, as well as potential targets for the most beneficial areas to treat for prevention of such scenarios. Though there are currently no such treatments to aid in areas that are likely to develop atherosclerosis, as is often the case with medical device innovations, as the diagnosis and understanding of a disease is better understood, so to can treatments be designed to meet these challenges.

Many advances must be made before such examples can come to fruition however. The continued advances in CT, magnetic resonance imaging (MRI), combined fluoroscopy/MRI machines, and other imaging modalities continue to allow for more accurate representations of the geometries of interest, while also holding the potential of accurate patient specific boundary conditions that are central to realistic CFD results.

Also important are tools for preparing the geometries for CFD from these imaging outputs. Numerous challenges still exist for fully automated segmentation, smoothing, of the models, as well as the meshing of the geometry. Future work improving the imaging modalities will positively affect our ability to rapidly obtain accurate representations of the anatomy and patient specific boundary conditions using completely non-invasive techniques. Advances in computer processing power, computational fluid dynamic methods and schemes for both the meshing and solving of CFD models will aid in the automation and speed with which future CFD analysis can be performed.

The multi-disciplinary approach will continue to be crucial in working through these challenges and enabling the future success of such endeavors. In fact, the importance of taking the needs of the physician, such as minimal required input, and of the patient, such as how a particular treatment might impact the patient's overall lifestyle into account, will become even more important as the challenges of today are met tomorrow.

<div align="center">

CURRICULM VITAE
Joseph A. Knight
joe@docknight.com

</div>

Education

07/2006 – 07/2009	**Swiss Federal Institute of Technology (ETH):** Zurich – Switzerland PhD Biomedical Engineering
01/2008 – 05/2009	**ETH Zurich Department of Technology Management (D-MTEC) (Additional Course Work)**

- General Management I
- General Management II
- Project Management

- Technology & Innovation Management
- Entrepreneurial Risk

09/2005 – 06/2006	**Stanford University:** Palo Alto, California - USA Biodesign Innovation Fellow
08/1998 – 04/2005	**University of South Florida (USF):** Tampa, Florida – USA M.S. Biomedical Engineering B.S. Engineering Science Certificate in Technology Entrepreneurship

Professional Experience

07/2006 – Present	**Swiss Federal Institute of Technology (ETH): Zurich - Switzerland** Research Engineer in biomedical engineering

- Engineered simple solutions to complex medical problems.
- Developed quantitative modeling and analysis tools to better understand and treat diseases of the heart.
- Collaborations and initiatives with multi-disciplinary group of individuals.

09/2005 – 06/2006	**Stanford University: Palo Alto, California - USA** Biodesign Innovation Fellow

- Through multi-disciplinary team collaboration, determined and solved pressing needs in healthcare – generated 8 patents awarded and pending.
- 1st place in the Silicon Valley Boomer Ventures business plan competition.
- Semi-finalist in the Business Association of Entrepreneurial Students (BASES) I-challenge business plan competition.
- Pitched winning business plan to Silicon Valley venture capitalists leading to founding of iRhythm Technologies.
- Externship at Guidant Cardiac Surgery (Boston Scientific); solved clinical need within 1 month period.

07/2005 - 06/2006	**The Foundry: Menlo Park, California - USA** *The Foundry, LLC is the premier medical device company incubator.* Engineering Consultant

- Performed background research on prior art, market, and clinical specifications for novel technology.
- Developed a computational & physical model to test the concept.

01/2005 - 06/2005	**Crosstree Capital Partners: Tampa, Florida - USA**

Crosstree is a leading Biotechnology industry-focused boutique Investment Firm.
Kauffman Entrepreneur Intern

- Analysed the Medical Device Industry to determine current market segments, trends, etc.
- Created taxonomic chart of industries segments, and after analysis of each, placed the 1600+ companies identified as significant to Crosstree's mission, into their respective area.

03/2004 - 06/2005	**USF Division of Patents & Licensing: Tampa, Florida - USA**

Marketing Specialist

- Analysed, patented, and marketed 100+ university technologies.
- Assisted in development of technologies through prior art search, marketability analysis and technology evaluation.

03/1996 - 03/2004	**53rd Infantry Brigade Florida Army National Guard: Orlando, Florida - USA**

Staff Sergeant

- Responsible for leadership and development of 50 soldiers.
- Led section and platoon to "Best Infantry T.O.W. Section" and "Best Infantry T.O.W. Platoon" in the 2/124th Infantry Battalion in 1999.
- Awarded Expert Infantryman's Badge (EIB) in 1999: Among the most highly prized peacetime decorations in the U.S. Army.
- Delta Company Soldier of Year in 1998 (1 of ~250).

Other Skills & Achievements

Awards/Honors	- 11 patents (4 awarded and 7 pending) - International Genetically Engineered Machine (iGEM) competition – led team to win best presentation at MIT – 2007 - Honorable mention *Best Paper in Conference*, International ANSYS/CFX Conference, Pittsburg, PA – 2004 - *Best Paper in Computational Fluid Dynamics Section*, International ANSYS/CFX Conference, Pittsburg, PA – 2004
Extracurricular	- Designed, implemented and taught course "The Process of Innovation" to students at the *Masinde Muliro of Science and Technology* (MMUST) in Kenya, Africa – 2008 to present - Completed 4 marathons – Zurich (3), Nairobi (1) - Completed solo and cross country flight requirements for single engine private pilot license – license pending final exam
Publications	- 10 business case studies and scientific manuscripts published - Chapter in *Surgery: Basic Science and Clinical Evidence 2nd* (Contributor)